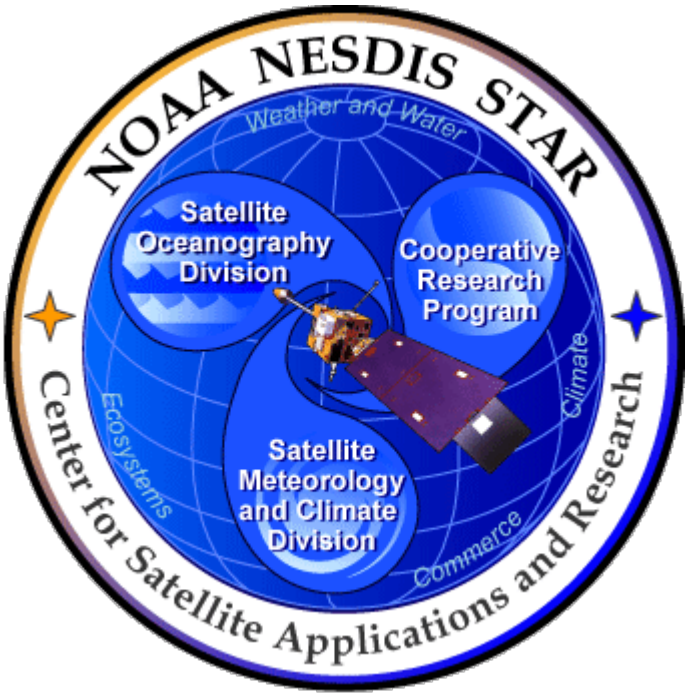

NOAA NESDIS

CENTER for SATELLITE APPLICATIONS and RESEARCH

GOES-R Advanced Baseline Imager (ABI) Algorithm Theoretical Basis Document

For Surface Albedo

Jingjing Peng, University of Maryland

Yunyue Yu, NOAA/NESDIS/STAR

Version 3

Sep 2020

VERSION HISTORY SUMMARY

Version	Description	Revised Sections	Date
0.1	New ATBD Document according to NOAA /NESDIS/STAR Document Guideline		8/30/2008
0.2	GOES-R Advanced Baseline Imager (ABI) Algorithm Theoretical Basis Document for Surface Albedo		9/30/2008
1.0	ATBD Document 80% readiness	Adding discussions on product uses in Section 2; Updating the newly developed algorithm in Section3; Providing validation results in Section 4; Supplementing more details in Sections 5 & 6	6/30/2010
2.0	ATBD Document 100% readiness	Describing the back-up algorithm; adding details on different paths to calculate BRF; providing graceful degradation strategies; updating with more validation results	6/12/2011
2.1	Corresponding to code version 6.0	Correcting and updating some information	12/1/2016
2.2	Corresponding to code version 7.0	Updating some information for QC and online processing outline	3/14/2017
2.2.1	Corresponding to code version 7.0	Correcting and updating some information	4/5/2017
2.2.2	Corresponding to code version 7.1	Add the startup setup and interruption control section; Updated the monitoring metadata list	2/22/2018

2.2.3	Corresponding to code version 7.1	Updated the metadata list and input instruction	3/23/2018
2.2.4	Corresponding to code version 7.2	Updated the description in Startup processing	04/12/2018
2.2.5	Corresponding to code version 7.3	Updated the description in Startup processing	05/20/2018
3.0	Corresponding to Framework code version v2r0 (The first integrated version in the operational system	Main updates include the cloud screening and subroutine selection criteria in online process, and BRDF calibration by integrating BRDF climatology in offline optimization.	09/20/2020

Note: Authorship of this ATBD before version 3.0 also include *Shunlin Liang, Dongdong Wang, Tao He, Yi Zhang of University of Maryland.*

TABLE OF CONTENTS

Page

LIST OF FIGURES

Page

LIST OF TABLES

Page

LIST OF ACRONYMS

2D	Two Dimension
ABI	Advanced Baseline Imager
ACM	ABI Cloud Mask
AIT	Algorithm Integration Team
AOD	Aerosol Optical Depth
ASTER	Advanced Spaceborne Thermal Emission and Reflection Radiometer
ATBD	Algorithm Theoretical Base Document
AVHRR	Advanced Very High-Resolution Radiometer
BRDF	Bidirectional Reflectance Distribution Function
BRF	Bidirectional Reflectance Factor
ETM+	Enhanced Thematic Mapper Plus
FD	Full Disk
FPT	Focal Plane Temperature
GOES	Geostationary Operational Environmental Satellite
GS-F&PS	Ground Segment Functional and Performance Specification
L1B	Level 1B
LSA	Land Surface Albedo
LUT	Look Up Table
LZA	Local Zenith Angle
MFRSR	Multi-Filter Rotating Shadowband Radiometers
MISR	Multi-angle Imaging Spectroradiometer
MODIS	Moderate Resolution Imaging Spectroradiometer
MRD	Mission Requirement Document
MSG	Meteosat Second Generation
NCEP	National center for Environmental Prediction
NESDIS	National Environmental Satellite, Data, and Information Service
NOAA	National Oceanic and Atmospheric Administration
PAR	Photosynthetically Active Radiation
POLDER	Polarization and Directionality of the Earth's Reflectance
PQI	Product Quality Information

PSP	Precision Spectral Pyranometer
QF	Quality Flag
QC	Quality Control
SEVIRI	Spanning Enhanced Visible and Infrared Imager
SNR	Signal Noise Ratio
SPOT	Systeme pour l'Observation de la Terre
STAR	Center for Satellite Applications and Research
SURFRAD	SURFace RADiation network
SZA	Solar Zenith Angle
TOA	Top Of Atmosphere
UTC	Coordinated Universal Time
VIIRS	Visible/Infrared Imager /Radiometer Suite

ABSTRACT

This land surface albedo (LSA) Algorithm Theoretical Basis Document (ATBD) provides a high level description and the physical and theoretical basis for the estimation of LSA with images taken by Advanced Baseline Imager (ABI) onboard the Geostationary Environmental Operational Satellite (GOES) R and S series of National Oceanic and Atmospheric Administration (NOAA) geostationary meteorological satellites. LSA is defined as the ratio between outgoing and incoming irradiance at the earth surface, which is a key component of surface energy budget. Besides the blue-sky broadband shortwave albedo, the LSA algorithm also generates spectral land surface reflectance as byproducts. The frequent temporal refreshment, fine spectral resolution and large spatial coverage make ABI a unique data source for mapping LSA. The ABI LSA algorithm combines atmospheric correction and surface Bidirectional Reflectance Distribution Function (BRDF) modeling in one optimization step to estimate BRDF parameters for each band. In order to improve computational efficiency, the ABI LSA algorithm is separated into the offline mode and the online mode. The routine offline mode is carried out at the end of each day, using a time series of clear-sky observations up to the current day to estimate BRDF parameters for the next days' online mode. In the online mode, LSA and surface reflectance products are produced in real-time. The direct estimation approach of albedo is implemented as the back-up algorithm when the routine offline algorithm fails. The ABI LSA algorithm has been tested and validated using satellite data. Comparison with field measurements shows our algorithm can satisfy the requirements of the GOES-R Ground Segment Functional and Performance Specification (F&PS).

1 INTRODUCTION

The purpose, users, scope, related documents and revision history of this document are briefly described in this section. Section 2 gives an overview of the Advanced Baseline Imager (ABI) Land Surface Albedo (LSA) algorithm derivation objectives and operation concept. Section 3 describes the LSA algorithm, its input data requirements, the theoretical background, mathematical descriptions and output of the algorithm. Some test results will be presented in Section 4. Practical considerations are described in Section 5, and followed by Section 6 on assumptions and limitations. Finally, Section 7 presents the references cited.

1.1 Purpose of This Document

The LSA Algorithm Theoretical Basis Document (ATBD) provides a high level description and the physical basis for the estimation of land surface albedo with images taken by ABI onboard the Geostationary Environmental Operational Satellite (GOES) R and S series of NOAA geostationary meteorological satellites. The LSA is a key parameter controlling surface radiation and energy budgets. LSA and land surface reflectance are also needed by other algorithms, such as snow coverage and radiation flux products.

1.2 Who Should Use This Document

The intended users of this document are those interested in understanding the physical basis of the algorithms and how to use the output of this algorithm to optimize the albedo estimate for a particular application. This document also provides information useful to anyone maintaining or modifying the original algorithm.

1.3 Inside Each Section

This document is subdivided into the following main sections:

- **System Overview**: Provides relevant details of the ABI and a brief description of the products generated by the algorithm.

- **Algorithm Description**: Provides a detailed description of the algorithm including its physical basis, its input, and its output.

- **Test Data Sets and Output**: Provides a description of the test data sets for characterizing the performance of the algorithm and quality of the data products. It also describes the results from algorithm processing using simulated input data.

- **Practical Considerations**: Provides an overview of the issues involving in numerical computation, programming and procedures, quality assessment and diagnostics and exception handling.

- **Assumptions and Limitations**: Provides an overview of the current limitations of the approach and gives the plan for overcoming these limitations with further algorithm development.

1.4 BRF and BRDF

Bidirectional reflectance factor (BRF) and bidirectional reflectance distribution function (BRDF) are two concepts that will be used frequently in this document. BRF is one kind of reflectance, a ratio between outgoing radiance at one given direction and incoming radiance at another given direction (same or different from the incoming direction). The reflectance byproduct of the LSA algorithm is the product of BRF. Surface reflectance and BRF are used interchangeably in this document. BRDF is a model to describe the bi-directional properties of reflectivity. In this document, BRDF is also used in the term "BRDF parameters" to refer to the kernel coefficients of the BRDF model.

1.5 Related Documents

LSA is one product of ABI product streamlines. The requirements of LSA products can be found in the specifications of the GOES-R Ground Segment Functional and Performance Specification (F&PS). LSA also requires other ABI products as the algorithm input. The readers can refer to these specific ATBDs for more information:

- *GOES-R Algorithm Theoretical Base Document for ABI Aerosol Optical Depth*
- *GOES-R Algorithm Theoretical Base Document for ABI Cloud Mask*

More references about the algorithm details are given in Section 5.

1.6 Revision History

Version 0.2 of this document was created by Drs. Shunlin Liang and Kaicun Wang of the Department of Geographical Science, University of Maryland, College Park and Dr. Yunyue Yu of NOAA NESDIS, Center for Satellite Applications and Research, Camp Springs, Maryland. According to the reviewers' comments, version of 1.0 was updated by Drs. Shunlin Liang and Dongdong Wang of the Department of Geographical Science, University of Maryland, College Park, and Dr. Yunyue Yu of NOAA. Refinement of the algorithm and latest validation results are updated in the Version 2.2 by Drs. Shunlin Liang, Dongdong Wang, Tao He and Mr. Yi Zhang of the Department of Geographical Science, University of Maryland, College Park, and Dr. Yunyue Yu of NOAA. Sartup set up and interruption control, metadata list and input data control are updated in the version 2.2 by Dr. Yunyue Yu of NOAA, and Dr. Jingjing Peng of the Earth System Science Interdisciplinary Center, University of Maryland, College Park. In response of the snow fraction user feedback to revise the snow reflectance, the online process and version 3 updated by Dr. Jingjing Peng and Dr. Yunyue Yu of NOAA of the Earth System Science Interdisciplinary Center, University of Maryland, College Park.

2 OBSERVING SYSTEM OVERVIEW

This section describes the products generated by the ABI LSA algorithm and the requirements it places on the sensor.

2.1 Products Generated

This albedo algorithm is responsible for estimation of LSA and land surface BRF for clear sky pixels identified by the ABI Cloud Mask (ACM) product. Using the ABI Aerosol Optical Depth (AOD) product as the first guess, this algorithm updates AOD and estimates AOD at points where ABI AOD products are not available, and then retrieves the parameters of the land surface BRDF model and derive LSA and land surface BRF values. It also incorporates albedo and BRDF climatology from previous satellite products (MODIS) as prior knowledge. Full disk blue-sky broadband albedo for the solar zenith angle smaller than 67° is produced. As a byproduct, full disk surface BRFs at the five visible and near-infrared bands are generated as well.

The surface albedo/reflectance product requirements defined by the Mission Requirement Document (MRD) and the Ground Segment Functional and Performance Specification (GS-F&PS) (NOAA 2009) are listed in Tables 2.1 and 2.2.

Table 2.1. GOES-R mission requirements for surface albedo product

Observational Requirement	Geographic Coverage[2]	Horiz. Res.	Mapping Accuracy	Msmnt. Range (albedo unit)	Msmnt. Accuracy (albedo unit)	Msmnt. Precision	Refresh Rate	Data Latency	Long-term Stability	Exent Qualifier
Albedo: Full Disk	FD	2 km	2 km	0 to 1	0.08	10%	60 mins	<2000 secs	TBD	LZA <70

Table 2.2. GOES-R mission requirements for surface reflectance product

Observational Requirement	Geographic Coverage[2]	Horiz. Res.	Mapping Accuracy	Msmnt. Range	Msmnt. cAccuray	Msmnt. Precision	Refresh Rate	Data Latency	Long-term Stability	Extent Qualifier
Reflectance: Full Disk	FD	2 km	2 km	0 to 2	0.08	0.08	60 mins	<2000 secs	TBD	LZA <70

As the key component of surface energy budget, satellite albedo products can be used to drive/calibrate/validate climatic, mesoscale atmospheric, hydrological and land surface models. Variation of LSA is also an important indicator of land cover and land use change. Analysis of long-term reliable albedo products will help better understand the human

dimension of climate change and how the vegetation-albedo-climate feedbacks work. The land surface reflectance byproducts will be the input to a number of other high-level land surface products, such as the factional snow cover product.

2.2 *Instrument Characteristics*

The LSA product is produced from clear-sky pixels observed by the ABI. The final channel set is still being determined as the algorithms are developed and validated. Table 2.3 highlights the ABI channels used by the albedo algorithm.

Table 2.3.Spectral characteristics of Advanced Baseline Imager

Channel Number	Central Wavelength (μm)	Bandwidth (μm)	Spatial Resolution
1	0.47	0.45 – 0.49	1 km
2	0.64	0.59 – 0.69	0.5 km
3	0.86	0.85– 0.89	1 km
4	1.38	1.37 – 1.39	2 km
5	1.61	1.58 – 1.64	1 km
6	2.26	2.23 – 2.28	2 km
7	3.9	3.80 – 4.00	2 km
8	6.15	5.77 – 6.60	2 km
9	7.0	6.75 – 7.15	2 km
10	7.4	7.24 – 7.44	2 km
11	8.5	8.30 – 8.70	2 km
12	9.7	9.42 – 9.80	2 km
13	10.35	10.10 – 10.60	2 km
14	11.2	10.80 – 11.60	2 km
15	12.3	11.80 – 12.80	2 km
16	13.3	13.00 – 13.60	2 km

Shaded channels are used for Albedo production.

3 ALGORITHM DESCRIPTION

This section provides a complete description of the algorithm, including both theoretical basis and technical details.

3.1 Algorithm Overview

Three steps are typically required to estimate the surface albedo from satellite multispectral TOA observations (Liang 2004; Schaaf et al. 2008):

(1) atmospheric correction,

(2) surface directional reflectance modeling,

(3) narrowband-to-broadband conversion.

The typical example is the MODIS surface albedo algorithm. The first step converts TOA reflectance into surface reflectance, the second step converts surface spectral reflectance into spectral albedos (individual ABI bands), and the last step converts spectral albedos to a broadband albedo. Instead, we propose an optimization method similar to the earlier algorithm used on the Meteosat data (Pinty et al. 2000a, b) to directly retrieve surface BRDF parameters, and then use the derived BRDF parameters to calculate LSA and land surface BRF. A similar strategy was also used to retrieve daily aerosol and surface reflectance simultaneously from the Spinning Enhanced Visible and Infrared Imager (SEVIRI) on the Meteosat Second Generation (MSG) (Govaerts et al. 2010; Wagner et al. 2010). Our proposed algorithm combines atmospheric correction and surface BRDF modeling together in one optimizing code (He et al. 2012). The optimization process estimates the BRDF parameters by minimizing a cost function considering both TOA reflectance and albedo climatology. Our revision over the previous methods mainly includes:

- AOD can vary over time;
- we use multiple ABI spectral channels enabling accurate production of shortwave broadband albedo;
- we use a different formulation of the atmospheric radiative transfer and surface BRDF model; and
- we incorporate albedo climatology as the constraint of optimization.

Both our optimization algorithm and traditional MODIS algorithm need aggregation of multiple clear-sky observations within a relatively short time periods, during which the surface conditions keep relatively stable. Continuous cloud coverage and rapidly changing surface usually cause the failure of the routine LSA algorithm. To handle these cases, we use the direct estimation approach as the back-up algorithm.

3.2 Processing Outline

3.2.1 Routine processing outline

The retrieval of BRDF parameters needs multiple observations over varied observing geometries. Since ABI is not a multi-angular sensor, we achieve this by using a stack of time series observations over each pixel within a short period time and assume the BRDF parameters are relatively stable during 14 days. The BRDF database is updated daily and the BRDF retrieval only needs one day's input. However, due to the cloud contamination and angle restriction, we accept the nearest TOA reflectance from the nearest available observation within 14 days.

The organization of time series data and retrieval of BRDF parameters are a time-consuming process. In order to improve the code efficiency, we divide our algorithm into two parts: the offline mode and the online mode. At the end of each day, an offline mode computation is conducted to perform a full inversion of BRDF parameters using the stacked time series data at 1-hour intervals. The calculated BRDF parameters are saved for the usage of the online mode next day ideally. To increase the robustness and continuity of the operational product, the LSA online algorithm accepts the latest BRDF parameters within one week as input.

When the routine algorithm based on successful BRDF retrieval fails, the back-up algorithm called direct estimation approach will be invoked to calculate broadband albedo directly in the online mode. Otherwise, the pre-calculated BRDF parameters are used to derive full disk LSA products every 60 minutes in the online mode. In addition to albedo, surface BRF will also be generated every 60 minutes in the online mode using AOD. Although ABI has a refreshing rate of 15 mins, surface albedo products are required to be generated every 60 mins. The online mode will select observation closest to each exact hour to calculate LSA and BRF. The processing chains of the LSA algorithm offline and online modes are shown in the Figures 3.1 and 3.2, respectively.

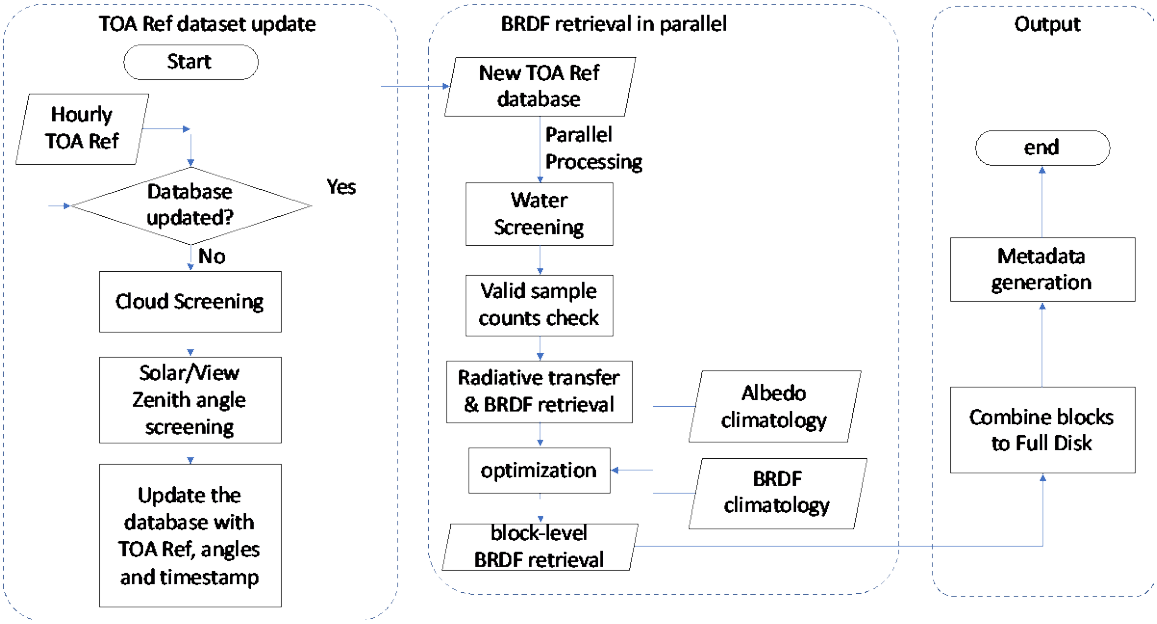

Figure 3.1. High level flowchart of the offline mode of ABI LSA algorithm, which is executed once at the end of each day to estimate the BRDF parameters.

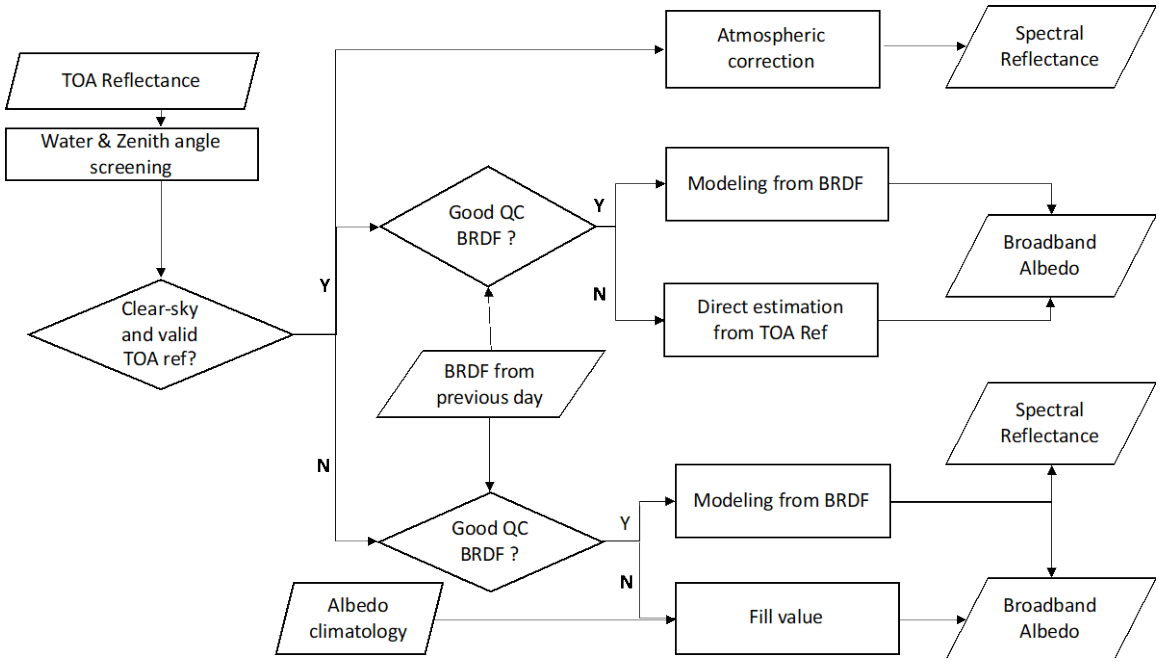

Figure 3.2. High level flowchart of the online mode of ABI LSA algorithm, illustrating the main processing components.

The LSA algorithm will take the ABI AOD product as one input when it is valid for accurate LSA estimation. For bright surface types or other conditions where the ABI AOD products are not available, the AOD information will be solely obtained from the LSA algorithm or filled.

3.2.2 Startup setup and interruption control

Automatic control handling strategy needs to be designed in case of systematic exceptions. For instance, the offline algorithm relies on an accumulation of clear-sky TOA observations to composite the BRDF. The timeliness of the TOA reflectance will influence the BRDF accuracy, so is necessary to consider how to deal with TOA data missing or system interruptions. Besides, the BRDF optimization algorithm needs reliable initial value input to improve the efficiency and effectiveness. When the BRDF from the climatology is available, it can provide the initial value for the optimization. Otherwise, the algorithm will switch to an experienced initial value and broader searching range to achieve the globally optimized coefficients. The applied exception handling strategy is introduced in this section, which also guides the setup method for a startup status of the NRT operation.

1) Data availability oriented branches

The online albedo/Reflectance retrieval requires the offline produced BRDF as input. The BRDF retrieval relies on an accumulation of TOA reflectance within a composition period. Normally, one days' FD observations have enough angle diversity to drive the BRDF retrieval. However, due to the cloud contamination and the geometry angle restriction, many pixels are still lack of sufficient reflectance observations after one day. Then the latest available clear-sky TOA reflectances work as a substitute. However, the time gap cannot be longer than 14 days so that the assumption of BRDF stability remains valid.

Thus each set-up process start with an accumulation of database for 10 days to make sure clear-sky TOA reflectance dataset available for most pixels. Before the completion of this spin-up period, the BRDF retrival sub-module will not be executed (Figure 3.3).

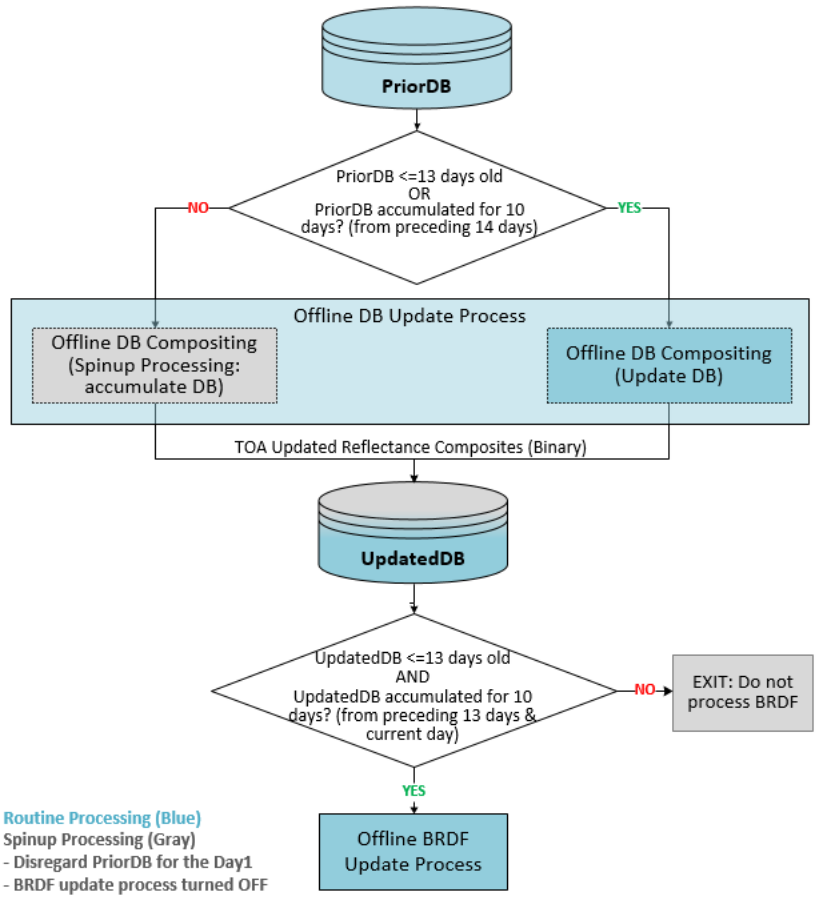

Figure 3.3 Daily calling procedure of offline procedures (DB refers to 'Database')

2) Seed data handling strategy

The offline algorithm deploys an optimization process to estimate the BRDF parameters. The BRDF climatology acts as an initial value in the optimization process accompanying and supplies the searching range in the response surface of the objective function, which will help accelerate the convergence. Otherwise, if the BRDF climatology is not available, the algorithm uses an experienced initial

value and a wider searching range in the response surface. According to our test, both situations will reach the global optimum with adequate input datasets. However, the latter will cost longer running time. The initial values and searching range of BRDF coefficients are listed in Table 3.2. The AOD uses a fixed initial value 0.1 and a search range of [0.01, 0.24],

Table 3.2 The optimization parameter setting about coefficients.

	f_{iso}		f_{vol}		f_{geo}	
	initial	range	initial	range	initial	Range
with previous BRDF	$f_{iso\text{-}clm\text{-}mean}$	[$f_{iso\text{-}clm\text{-}min}$, $f_{iso\text{-}clm\text{-}max}$]	$f_{vol\text{-}clm\text{-}mean}$	[$f_{vol\text{-}clm\text{-}min}$, $f_{vol\text{-}clm\text{-}max}$]	$f_{geo\text{-}clm\text{-}mean}$	[$f_{geo\text{-}clm\text{-}min}$, $f_{geo\text{-}clm\text{-}max}$]
without previous BRDF	0.2	[0,1]	0.1	[0,0.4]	0.05	[0,0.1]

3.3 Algorithm Input

This section describes the input required to execute the LSA algorithm. The offline mode and online mode have different requirements. Tables 3.3 and 3.4 list them respectively.

The input data selection criteria for offline dataset update include:

- Ten hourly observations are required for each day's database update.
- If the data at the exact hour is not available, the closest time stamp (outreach by no more than half hour at each end) can be used as long as all the input data are at the same time. The time stamp does not need to be the same over different days. For example, DOY1 1215, DOY2 1200, are good to use.
- A complete set of the dynamic input data (L1B bands, navigation and cloud mask) are required for each hourly time-steps. If any one of the data file is found missing, observations for that timestamp should not be used.

Table 3.3. Summary of inputs for ABI LSA algorithm offline mode.

Sensor input (One day's data)	TOA reflectance at five bands
	View zenith angle
	Solar zenith angle
	View azimuth angle
	Solar azimuth angle

		Navigation (Geolocation, water mask)
Ancillary data	**ABI products (One day's data)**	Cloud mask
	Non-ABI static data	Surface albedo climatology
		BRDF climatology
		Atmosphere LUT
	Intermediate dynamic data	Clear-sky Observation Database
		BRDF and its QC of previous day
		Configuration file

Table 3.4. Summary of inputs for ABI LSA algorithm online mode.

Sensor input (Current timestamp)		TOA reflectance at five bands
		View zenith angle
		Solar zenith angle
		View azimuth angle
		Solar azimuth angle
		Navigation (Geolocation, Water mask)
Ancillary data	**ABI products (Current timestamp)**	Aerosol optical depth
		Cloud mask
	Non-ABI static data	Surface albedo climatology
		Atmosphere LUT
		Coefficients of direct estimation for albedo
	Intermediate dynamic data	Pre-calculated BRDF parameters
		IMS snow mask
		Configuration file

Basically, the offline mode algorithm needs the time series of all types of input data and the online mode involves only the data sets closest to the current observation hour since the online mode algorithm is only run once an hour. Moreover, the online mode needs the pre-calculated BRDF parameters as the input. For one particular data set, the online mode and offline mode share the same details, which are given in the following subsections.

3.3.1 Primary Sensor Data

Primary sensor data is information that is derived solely from the ABI observations. The primary sensor data used by the LSA algorithm include both the TOA reflectance values and relevant ancillary information (angles, geolocation, and land/water mask). The spatial resolution of LSA and BRF products are 2km, the input ABI sensor data should be aggregated to 2km as well.

The L1B reflectance sensor quality check (Criterion refer to Table 5.1.3.6.3 and Table 5.1.3.6.4 in GOES R SERIES PUG vol3) uses the 4-level DQF layer in ABI L1B data together with the TOA reflectance value: if the DQF is equal to 0 (good_pixel_qf) and the reflectance value is within [0,1], then the pixel quality is regarded as good, otherwise, it is regarded as bad pixel.

Table 3.5. Input list of primary sensor data.

Name	Type	Description	Dimension
Ch1	input	Calibrated ABI level 1b reflectance at channel 1	grid (xsize, ysize)
Ch2	input	Calibrated ABI level 1b reflectance at channel 2	grid (xsize, ysize)
Ch3	input	Calibrated ABI level 1b reflectance at channel 3	grid (xsize, ysize)
Ch5	input	Calibrated ABI level 1b reflectance at channel 5	grid (xsize, ysize)
Ch6	input	Calibrated ABI level 1b reflectance at channel 6	grid (xsize, ysize)
Latitude	input	Pixel latitude	grid (xsize, ysize)
Longitude	input	Pixel longitude	grid (xsize, ysize)
Solar zenith	input	ABI solar zenith angles	grid (xsize, ysize)
Solar azimuth	input	ABI solar azimuth angles	grid (xsize, ysize)
View zenith	input	ABI view zenith angle	grid (xsize, ysize)
View azimuth	input	ABI view azimuth angle	grid (xsize, ysize)
Land/water mask	input	ABI land/water mask	grid (xsize,ysize)

3.3.2 Derived Sensor Data

There are two ABI derived sensor data products required by the LSA algorithm: 1) the ABI Cloud Mask (ACM) product, which indicates four cloudiness states for each pixel: clear, probably clear, probably cloudy, and cloudy, and 2) the ABI AOD. The algorithm has

separate retrieving strategies for clear-sky and cloudy pixels, recognized using the cloud mask input. The pixels with cloud mask of 0 (Absolutely clear) and 1 (Probably clear) are retrieved through the clear-sky subroutine.

Table 3.6. Input list of derived sensor data.

Name	Type	Description	Dimension
Cloud mask	input	ABI cloud mask product	grid (xsize, ysize)
AOD	input	ABI AOD product	grid (xsize, ysize)

3.3.3 Ancillary Data

Ancillary data are data other than the ABI sensor and derived data (Table 3.7). The following lists and briefly describes the ancillary data required to run the LSA algorithm.

- **IMS snow mask data**

  The IMS snow mask data is used to determine the snow condition for each pixel.

- **LSA Climatology**

  The albedo climatology includes the mean and variance of land surface spectral and broadband albedos. The albedo climatology will be used as the background values in the albedo estimation. Multiple years' MODIS albedo products are averaged and used as climatology. The MODIS albedo climatology is calculated at 8-day intervals.

- **BRDF Climatology**

  The BRDF climatology provides the prior knowledge about mean, max, min, and std of each BRDF parameter in a specific day of year. The BRDF climatology supplies 'primary guess' and search range of BRDF coefficients in the optimization algorithm.

- **Look-Up table**

  In order to improve the computational efficiency, the atmospheric parameters have been pre-calculated using the 6S simulation and stored into the look-up table (LUT). LUT is a type of static input to the algorithm and all codes share the same set of LUT. The parameters in the LUT include:

  - Atmospheric intrinsic reflectance

- Total global gas transmittance
- Downward total scattering transmittance
- Upward total scattering transmittance
- Total spherical albedo
- Optical depth
- Direct irradiance ratio

After a sensitivity analysis, we select the entries of our LUT by balancing the accuracy and the computational efficiency (Table 3.8).

- **BRDF model parameters**

  BRDF model parameters are useful for integrating albedo. The parameters are the output of the offline mode code and also the input of the online mode code.

- **Coefficients of direct estimation approach**

  Two groups of coefficients to calculate black-sky and white-sky albedo respectively from TOA spectral reflectance are stored for each observing geometry. The intervals for viewing geometries are the same as used in the LUT (Table 3.8).

Table 3.7 Input of ancillary data.

Name	Type	Description	Dimension
Land/water mask	Input	A land-water mask	grid (xsize, ysize)
Albedo climatology	Input	MODIS multiple years' mean	grid (xsize, ysize), 46 granules in a year
BRDF climatology	Input	Historical mean, maximum, minimum, and standard deviation of each BRDF parameter	grid (xsize, ysize), 366 granules in a year
Atmosphere LUT	Input	Seven atmospheric parameters as function of aerosol model, aerosol optical depth, ABI channel and observing geometry	(16x 16 x 7 x 10 x 5)*
Coefficient of direct estimation approach	Input	Two groups of coefficients for calculating black-sky and white-sky albedo respectively for each observing geometry	(16x 16 x 7 x 6 x 2)
BRDF parameters	Input	Ch1 f_iso: BRDF isotropic component parameter at Ch1	grid (xsize, ysize)

		Ch1 f_vol: BRDF volumetric kernel parameter at Ch1	grid (xsize, ysize)
		Ch1 f_geo: BRDF geometric kernel parameter at Ch1	grid (xsize, ysize)
		Ch2 f_iso: BRDF isotropic component parameter at Ch2	grid (xsize, ysize)
		Ch2 f_vol: BRDF volumetric kernel parameter at Ch2	grid (xsize, ysize)
		Ch2 f_geo: BRDF geometric kernel parameter at Ch2	grid (xsize, ysize)
		Ch3 f_iso: BRDF isotropic component parameter at Ch3	grid (xsize, ysize)
		Ch3 f_vol: BRDF volumetric kernel parameter at Ch3	grid (xsize, ysize)
		Ch3 f_geo: BRDF geometric kernel parameter at Ch3	grid (xsize, ysize)
		Ch5 f_iso: BRDF isotropic component parameter at Ch5	grid (xsize, ysize)
		Ch5 f_vol: BRDF volumetric kernel parameter at Ch5	grid (xsize, ysize)
		Ch5 f_geo: BRDF geometric kernel parameter at Ch5	grid (xsize, ysize)
		Ch6 f_iso: BRDF isotropic component parameter at Ch6	grid (xsize, ysize)
		Ch6 f_vol: BRDF volumetric kernel parameter at Ch6	grid (xsize, ysize)
		Ch6 f_geo: BRDF geometric kernel parameter at Ch6	grid (xsize, ysize)

* The LUT dimension corresponds to num_solar_zenith_angle * num_sensor_senith_angle * num_relative_azimuth_angle * num_aerosol_optical_depth * num_bands

Table 3.8 Entries of LUT.

Entries to LUT	Values
Solar Zenith Angle	0.,5.,10.,15.,20.,25.,30.,35.,40.,45.,50.,55.,60.,65.,70.,75.
Sensor Zenith Angle	0.,5.,10.,15.,20.,25.,30.,35.,40.,45.,50.,55.,60.,65.,70.,75.
Relative Azimuth Angle	0., 30., 60., 90., 120., 150., 180.
Aerosol Optical Depth	.01,.05,.1,.15,.2,.3,.4,.6,.8,1.

- **Clear-sky observation database**

The database stores the clear-sky observations for each day hour during a day (10 in total, 12~21 UTC for G-16, 14~23 UTC for G-17), observation closest to each exact hour will be used to build up the database. The clear-sky observation for each time step is collected from the available day closest to the current day. The time stamp and solar angular information will be stored as well into the database. This database will be updated each day by absorbing the newest clear-sky observations with the time stamp and solar angular information (Table 3.9).

The database includes both inputs and outputs of the offline mode calculations. At the end of each day, the offline code examines all the new observations and updates the database. This maintenance procedure in the offline mode mainly conducts the following steps iterating over each pixel for each timestamp:

1) read in the reflectance database and set the time step T_i to the beginning of the day (T_0);
2) read in the TOA reflectance data the corresponding cloud mask at time step T_i;
3) check the observing geometries: if the sensor zenith is larger than 70° or the solar zenith is larger than 67°, the old data in the database will be kept go to Step 2) for the next time stamp T_{i+1}; otherwise continue with Step 4) for time step T_i;
4) check if the pixel is cloud contaminated (cloud present or cloud shadow present) according to the cloud mask and other constraints on spectral reflectance: if yes, the old data in the database will be kept and go to Step 2) for the next time stamp T_{i+1}; otherwise continue with Step 5) for time step T_i;
5) check if the L1B observations have good quality (criterion refer to Table 5.1.3.6.3 and Table 5.1.3.6.4 in GOES R SERIES PUG vol3) using the 4-level DQF layer in ABI L1B data and the reflectance value: if the DQF is not equal to 0 (good_pixel_qf) or the reflectance value is beyond [0 1], the old data in the database will be kept and go to Step 2) for the next time stamp T_{i+1}; otherwise continue with Step 6) for time step T_i;
6) update the database with the current TOA reflectance, together with its corresponding angles and acquisition time;
7) Continue with the next time stamp T_{i+1} from Step 2) until the end of the day.

Table 3.9 Details of Clear-sky observation database

Name	Type	Description	Dimension
Ch1	input	Calibrated ABI level 1b reflectance at Ch1	grid (xsize, ysize, T_i)
Ch2	input	Calibrated ABI level 1b reflectance at Ch2	grid (xsize, ysize, T_i)

Ch3	input	Calibrated ABI level 1b reflectance at Ch3	grid (xsize, ysize, T_i)
Ch5	input	Calibrated ABI level 1b reflectance at Ch5	grid (xsize, ysize, T_i)
Ch6	input	Calibrated ABI level 1b reflectance at Ch6	grid (xsize, ysize, T_i)
Solar zenith	input	ABI solar zenith angles	grid (xsize, ysize, T_i)
Relative azimuth	input	ABI relative azimuth angles	grid (xsize, ysize, T_i)
Time stamp	input	Julian day of the clear-sky observation at T_i	grid (xsize, ysize, T_i)

3.4 Theoretical Description

After analyzing existing albedo algorithms, we proposed an ABI LSA algorithm similar to the earlier algorithm used on Meteosat data (Pinty et al. 2000a, b) and the approach tested on MSG/SEVIRI data (Govaerts et al. 2010; Wagner et al. 2010). The albedo algorithm from the geostationary Meteosat observations combined atmospheric correction and BRDF modeling by assuming one unknown constant AOD for the whole period of time (daily). Here, we made several major revisions. For example, AOD can vary over time, and multiple ABI spectral bands enable production of broadband albedo. In addition, the formulation of the atmospheric radiative transfer and surface BRDF model are also different.

This optimization approach will serve as the routine algorithm to derive BRDF parameters in the offline mode (Section 3.4.1). The next section describes the mathematical foundation and procedures used in the online mode.

3.4.1 The offline mode

The critical step in retrieving LSA and land surface BRF is to estimate the surface BRDF parameters. This procedure is time-consuming and carried out once each day in the offline mode. The tasks of the offline mode mainly include: 1) maintenance of clear-sky TOA reflectance database, and 2) retrieval of BRDF parameters using this database. The first task deals mainly with data I/O, and the programing procedure has been briefly introduced in Section 3.3.3 and will not be discussed here. The second part is the core of the LSA routine algorithm and will be introduced in details here. The mathematical equations used in the retrieval of BRDF parameters are given in Section 3.4.1.1. Section 3.4.1.2 discusses how to optimize and derive spectral BRDF parameters from TOA database using these equations.

3.4.1.1 **Mathematical formulation**

In order to obtain BRDF parameters, we need to execute the atmospheric correction and BRDF modeling. A traditional way (e.g. the MODIS albedo algorithm) to achieve this is to implement them separately in two steps. Here, we achieve this in one step by combining both the atmospheric radiative transfer process and BRDF modeling in our optimization

schema. Three groups of equations are introduced here: the BRDF model, the Atmospheric radiative transfer equations, and equations calculating albedo from BRDF parameters.

3.4.1.1.1 Land surface BRDF model

Performance of albedo retrieval from satellite observations is usually restricted by a limited sampling of directional surface reflectance. Therefore, a model is usually used to characterize the surface anisotropy. The model can be inverted with a finite set of angular samples and used to calculate surface reflectance in any sun-view geometry and to derive surface albedo. An empirical kernel-based BRDF model will be used in the ABI LSA algorithm.

Maignan et al. (2004) found that among the current BRDF models, the best two are the three-parameter linear Ross–Li model and the nonlinear Rahman–Pinty–Verstraete model. However, all models fail to accurately reproduce the sharp reflectance increase close to the backscattering (hotspot peak) direction. Based on physical considerations, Maignan et al. (2004) suggested a modification of the Ross–Li model, without the addition of a free parameter, to account for the complex radiative transfer within the land surfaces that leads to the hot spot signature. They illustrated that the modified linear model performs better than all others.

The modified three-parameter linear Ross–Li BRDF model can be written as (Maignan et al. 2004):

$$r_{dd}(\theta_s,\theta_v,\phi) = f_{iso} + f_{vol}\cdot K_{vol}(\theta_s,\theta_v,\phi) + f_{geo}\cdot K_{geo}(\theta_s,\theta_v,\phi) \tag{1}$$

where the volumetric and geometrical kernel function has the following form:

$$K_{vol} = \frac{(\pi/2-\xi)\cos\xi + \sin\xi}{\cos\theta_s + \cos\theta_v}\left(1 + \frac{1}{1+\xi/\xi_0}\right) - \frac{\pi}{4} \tag{2}$$

$$K_{geo} = O(\theta_s,\theta_v,\phi) - \sec\theta_s - \sec\theta_v + 0.5(1+\cos\xi)\sec\theta_s\sec\theta_v \tag{3}$$

and where

$$O = (t - \sin t\cos t)(\sec\theta_s + \sec\theta_v)/\pi \tag{4}$$

$$\cos t = \frac{h\sqrt{D^2 + (\tan\theta_s\tan\theta_v\sin\phi)^2}}{b(\sec\theta_s + \sec\theta_v)} \tag{5}$$

$$D = \sqrt{\tan^2\theta_s + \tan^2\theta_v - 2\tan\theta_s\tan\theta_v\cos\phi} \tag{6}$$

$$\cos\xi = \cos\theta_s\cos\theta_v + \sin\theta_s\sin\theta_v\cos\phi \tag{7}$$

and where ξ_0=0.026, $\frac{h}{b}$=2.0, and all the angles have the unit of radian.

3.4.1.1.2 Formulation of TOA reflectance

To retrieve AOD and the parameters of the surface BRDF from TOA reflectance, we have to establish TOA reflectance as a function of BRDF parameters and AOD. Here, we use the formulation proposed by Qin et al. (2001). The formula for TOA reflectance $\rho(\Omega_s,\Omega_v)$ is expressed as:

$$\rho(\Omega_s,\Omega_v)=\rho_0(\Omega_s,\Omega_v)+\frac{T(\Omega_s)R(\Omega_s,\Omega_v)T(\Omega_v)-t_{dd}(\Omega_s)t_{dd}(\Omega_v)\left|R(\Omega_s,\Omega_v)\right|\overline{\rho}}{1-r_{hh}\overline{\rho}} \tag{8}$$

where $\Omega_s\in(-\mu_s,\phi_s)$ is the solar incoming direction, and $\Omega_v\in(\mu_v,\phi_v)$ for the viewing direction. There are two groups of coefficients in the above expression that are independent of each other: atmosphere-dependent and surface-dependent. These coefficients in each group represent the inherent properties of either the atmosphere or the surface. This means that we can determine these two groups of coefficients separately.

For the atmosphere, $\rho_0(\Omega_s,\Omega_v)$ is the atmospheric reflectance associated with path radiance (zero surface reflectance), and $\overline{\rho}$ is the atmospheric spherical albedo as defined before. The transmittance matrices are defined as:

$$T(\Omega_s)=\left[t_{dd}(\Omega_s)\quad t_{dh}(\Omega_s)\right] \tag{9}$$

$$T(\Omega_v)=\left[t_{dd}(\Omega_v)\quad t_{hd}(\Omega_v)\right]^T \tag{10}$$

where the subscript T stands for transpose, each transmittance has two subscript symbols: d (directional) and h (hemispherical).

The direct transmittance (t_{dd}) has the simple analytical expression: $t_{dd}(\mu)=\exp(-\tau_t/\mu)$.

The directional-hemispheric transmittance (t_{dh}) defines the fraction of downward diffuse flux generated by atmospheric scattering as the direct beam passes through the atmosphere. It can be calculated as the ratio of the integrated sky radiance at the surface level $L^{\downarrow}(\Omega_s,\Omega_v)$ over the downward hemisphere to the TOA incoming solar radiation:

$$t_{dh}(\Omega_s)=\frac{\int_{2\pi^-}L^{\downarrow}(\Omega_s,\Omega_v)\mu_v d\Omega_v}{\mu_s F_0} \tag{11}$$

The hemispheric-directional transmittance (t_{hd}) is defined as the ratio of the integrated upwelling TOA radiance over the upper hemisphere to the upwelling flux at the surface level $F^{\uparrow}$:

$$t_{hd}(\Omega_v) = \frac{\int_{2\pi^+} L^{\uparrow}(\Omega_s, \Omega_v)\mu_s d\Omega_s}{F^{\uparrow}} \tag{12}$$

where both t_{dh} and t_{hd} have to be calculated numerically. A practical solution is to create look-up tables in advance.

For the surface, the reflectance matrix is defined as:

$$R(\Omega_s, \Omega_v) = \begin{bmatrix} r_{dd}(\Omega_s, \Omega_v) & r_{dh}(\Omega_s) \\ r_{hd}(\Omega_v) & r_{hh} \end{bmatrix} \tag{13}$$

where $r_{dd}(\Omega_s, \Omega_v)$ is the surface BRF. The directional-hemispherical reflectance $r_{dh}(\Omega_s)$ (or black-sky albedo) is defined as:

$$r_{dh}(\Omega_s) = \frac{1}{\pi}\int_{2\pi^+} r_{dd}(\Omega_s, \Omega_v) d\Omega_v\,, \tag{14}$$

where the integration is over the upper hemisphere. The hemispherical-directional reflectance $r_{hd}(\Omega_v)$ is defined in the same way, but the integration is over the lower hemisphere:

$$r_{hd}(\Omega_v) = \frac{1}{\pi}\int_{2\pi^-} r_{dd}(\Omega_s, \Omega_v) d\Omega_s \tag{15}$$

The bi-hemispherical reflectance (r_{hh})(or white-sky albedo)is:

$$r_{hh} = 2\int_0^1 r_{dh}(\mu_s)\mu_s d\mu_s \tag{16}$$

where $\mu_s = \cos(\theta_s)$.

The determinant $|R|$ is easily calculated as:

$$\left|R(\Omega_s, \Omega_v)\right| = r_{dd}(\Omega_s, \Omega_v) r_{hh} - r_{dh}(\Omega_s) r_{hd}(\Omega_v) \tag{17}$$

It is evident that as long as surface BRDF parameters are known, the surface reflectance matrix can be determined. The authors claim that this approach does not introduce any approximation into the formulation, and their numerical experiments demonstrate that this formulation is very accurate (Qin et al., 2001).

3.4.1.1.3 Calculation of albedos

After obtaining BRDF parameters, it is straightforward to calculate spectral black-sky albedo, which are simply integrations of the surface directional reflectance functions over the entire viewing hemisphere. The spectral albedos are denoted as narrowband albedos in the next section. Instead of directly carrying out the numeric integration, we calculate the integral using an empirical polynomial equation of the three kernel parameters, similar to the MODIS albedo algorithm (Schaaf et al. 2002), fitting black-sky albedo with a polynomial function:

$$\begin{aligned}\alpha_{bs}(\theta_s) &= f_{iso}a + f_{vol}(b_0 + b_1\theta_s + b_2\theta_s^{\,2} + b_3\theta_s^{\,3} + b_4\theta_s^{\,4} + b_5\theta_s^{\,5}) \\ &+ f_{geo}(c_0 + c_1\theta_s + c_2\theta_s^{\,2} + c_3\theta_s^{\,3} + c_4\theta_s^{\,4} + c_5\theta_s^{\,5})\end{aligned} \tag{18}$$

Where θ_s is the solar zenith angle, and $a, b_0, b_1, b_2, b_3, b_4, b_5, c_0, c_1, c_2, c_3, c_4, c_5$ are the regression coefficients, whose values are listed in Table 3.10. Similarly, the white-sky albedo can be computed by using the equation:

$$\alpha_{ws} = f_{iso}a + f_{vol}b + f_{geo}c \tag{19}$$

Table 3.10. Coefficients used to calculate albedo from BRDF parameters.

Variable	Value	Variable	Value
a	1.0	c_0	-1.2661
b_0	-0.0003	c_1	-0.4434
b_1	0.3368	c_2	2.2809
b_2	-1.7243	c_3	-4.8262
b_3	4.01077	c_4	3.9824
b_4	-3.4934	c_5	-1.1456
b_5	1.1442		
a	1.0		
b	0.2260		
c	-1.3763		

After the narrowband albedos are obtained from the integration of the directional reflectance model, narrowband to broadband conversions are carried out based on empirical statistical relationships. The broadband albedo mainly depends on surface spectral albedo spectra, but is also affected by the atmospheric conditions. With extensive radiative transfer simulations and surface reflectance spectral measurements, we have developed the conversion formulas for calculating the total shortwave albedo, total-, direct-, and diffuse-, visible, and near-infrared broadband albedos for several narrowband sensors (Liang 2001; Liang et al. 2003; Liang et al. 1999), including ASTER, AVHRR, GOES, Landsat-7 ETM+, MISR, MODIS, POLDER, and VEGETATION in SPOT spacecraft. A similar approach was later applied to generate the conversion formula for VIIRS (Liang et

al. 2005a). The formula for MODIS has been used for routine albedo production (Schaaf et al. 2002), the MISR formula for calculating shortwave albedo is very effective (Chen et al. 2008), and the VIIRS formula will be used for operational albedo production. The same strategy also will be used to covert five ABI narrowband albedos to one broadband albedo.

The broadband albedo can be converted from spectral albedos using the following empirical formula:

$$\bar{r}(\theta_s) = \beta_0 + \beta_1 F_1 r_1(\theta_s) + \beta_2 F_2 r_2(\theta_s) + \beta_3 F_3 r_3(\theta_s) + \beta_5 F_5 r_5(\theta_s) + \beta_6 F_6 r_6(\theta_s) \qquad (20)$$

where $r_i(\theta_s)$ are the spectral albedo, β_i are the coefficients, F_i are the normalized downward irradiance of the ABI five bands:

$$F_i = \frac{E_i(\theta_s)}{E_1(\theta_s) + E_2(\theta_s) + E_3(\theta_s) + E_5(\theta_s) + E_{6i}(\theta_s)} \qquad (21)$$

and are the downward irradiance of each band (at the specific solar zenith angle). Radiative transfer simulations and statistical analysis provide the coefficients β_i. The equations used for three sensors are given below:

$$\alpha_{MODIS} = 0.160\alpha_1 + 0.291\alpha_2 + 0.243\alpha_3 + 0.116\alpha_4 + 0.112\alpha_5 + 0.0713\alpha_7 - 0.0015$$

$$\alpha_{SEVIRI} = 0.4331\alpha_1 + 0.3939\alpha_2 + 0.1136\alpha_3 - 0.0084$$

$$\alpha_{ABI} = 0.2692\alpha_1 + 0.1661\alpha_2 + 0.3841\alpha_3 + 0.1138\alpha_5 + 0.0669\alpha_6$$

3.4.1.2 **Derivation of BRDF parameters**

Given the surface BRDF model (1) and the atmospheric radiative transfer model (8), the BRDF parameters and AOD at each observation can be obtained by minimizing the following cost function:

$$J(x) = (r(x) - r_b)B^{-1}(r(x) - r_b) + (\hat{\rho}(x) - \rho)R^{-1}(\hat{\rho}(x) - \rho) \qquad (22)$$

where $\boldsymbol{x}$ are the three coefficients of the surface BRDF model and AOD, $r(x)$ is the calculated white-sky surface albedo using the BRDF model, r_b are the "first-guess" values of albedo from albedo climatology, B is the uncertainty matrix of the albedo "first-guess" values, ρ is the observed ABI TOA reflectance, $\hat{\rho}$ is the calculated TOA reflectance from equation (8), and R is the error matrix of the calculated TOA reflectance.

In this cost function, r_b is from the albedo climatology, B and R are preset values; ρ is the observed TOA reflectance. Given one group of BRDF parameters, the white-sky surface albedo could be calculated easily (see Section 3.4.1.1.3). Given AOD in addition to BRDF parameters, the TOA spectral reflectance could be calculated from the Qin's radiative transfer equation (8) (see Section 3.4.1.1.2). In this optimization system, the parameters to be optimized are spectral BRDF parameters and AOD. There are many different approaches available to minimize the cost function and obtain the BRDF parameters. We employ the Shuffled Complex Evolution method (SCE-UA, Duan et al. (1992) and Duan et al. (1993)), an efficient algorithm in searching global optimals. The SCE-UA method is capable of handling high parameter dimensionality and it does not rely on the availability of an explicit expression for the objective function or the derivatives.

3.4.2 The online mode

According to the results of two tests (whether the offline mode returns successfully and whether clear-sky observations are available during the 60-minutes' window), the online mode chooses various paths to calculate albedos and BRFs. Here the clear-sky observations is required to be with good quality in L1B data. The cloud condition detection and the sensor quality check are performed at the same time.

The L1B reflectance sensor quality check (Criterion refer to Table 5.1.3.6.3 and Table 5.1.3.6.4 in GOES R SERIES PUG vol3) uses the 4-level DQF layer in ABI L1B data together with the TOA reflectance value. If the DQF is equal to 0 (good_pixel_qf) and the reflectance value is within [0,1], then the pixel quality is regarded as good; otherwise, it is regarded as bad pixel. The ABI cloud mask will be used for all cloud detection. Primary algorithms will be performed on each clear-sky (i.e. "Absolutely-clear" or "Probably clear" indicated by the 4-level cloud mask) surface pixel with good sensor quality.

3.4.2.1 **Calculation of albedos**

3.4.2.1.1 Routine algorithm

If the offline mode returns successfully, the online mode uses the retrievals of BRDF parameters from the offline mode to calculate albedos. This is called the routine algorithm. Using equations (18) and (19), we can obtain both black-sky and white-sky spectral albedos. The broadband black-sky and white-sky albedos could then be derived from Equation (21). Given the black-sky and white-sky broadband albedo, the blue-sky broadband albedo α can be calculated by:

$$\alpha = p\alpha_{ws} + (1-p)\alpha_{bs} \tag{23}$$

where p is the diffuse fraction of the total radiation. 1-p is the direct fraction of the total radiation. The fraction of direct irradiance is one parameters of the LUT. Given AOD, the corresponding p could be searched from the LUT. If no AOD value is available, the default value of 0.1 will be used in searching LUT.

3.4.2.1.2 Back-up algorithm

The routine optimization algorithm needs aggregation of multiple clear-sky observations within a relatively short time periods, during which the surface conditions keep relatively stable. Continuous cloud coverage and rapidly changing surface usually cause the failure of this algorithm. To handle these cases, we propose the direct estimation approach as the back-up algorithm (Liang 2003; Liang et al. 2002; Liang et al. 2005b). Unlike the optimization approach, the direct estimation approach uses only one set of clear-sky observations at one time as the input. Validation shows this approach could produce reliable albedos over both "dark" surfaces and "bright" surfaces. The Joint Polar Satellite System (JPSS) VIIRS albedo product has adopted this approach as the operational algorithm (Wang et al. 2013).

The mathematical formulation of this approach is not complicated. The extensive simulations of atmospheric radiative transfer show there exists good relationship between the surface albedo and TOA spectral reflectance, if the observing geometry is fixed. Instead of deriving BRDF parameters first and then calculating albedo from the BRDF parameters, the direct estimation approach directly calculate the surface albedo from TOA signals.

For a given combination of solar zenith angle θ_s, view zenith angle θ_v and relative azimuth angle φ, surface albedo α could be calculated from TOA spectral reflectance $\rho_i(\theta_s, \theta_v, \varphi)$ at five bands (i=1,2,3,5,6) using a linear equation:

$$\alpha = a_0(\theta_s, \theta_v, \varphi) + \sum_{i=1,2,3,5,6} a_i(\theta_s, \theta_v, \varphi)\rho_i(\theta_s, \theta_v, \varphi) \tag{24}$$

where $a_i(\theta_s, \theta_v, \varphi)$ (i=0,1,2,3,5,6) are preset coefficients dependent on viewing geometry.

The regression coefficients were derived offline through extensive simulations of atmospheric radiative transfer. Two groups of coefficients are stored to calculate white-sky albedo and black-sky albedo respectively.

3.4.2.1.3 Graceful degradation

If the offline mode returns successfully, instantaneous albedos could be calculated whether clear-sky observation is available or not. However, the back-up algorithm requires clear-sky observations as input. If no clear-sky observation is available and no BRDF parameters are retrieved, we have to find alternative to predict albedo, instead of providing filling values. Yang et al. (Yang et al. 2008) gave an empirical equation to calculate black-sky albedo α_{bs} from white-sky albedo α_{ws} when solar zenith angle θ is known:

$$\alpha_{bs} = \alpha_{ws} \frac{1+1.14}{1+1.48\cos\theta} \qquad (25)$$

We use this equation to predict instantaneous albedo from the climatological white-sky albedo for the case no clear-sky observation is available and no BRDF parameter is retrieved.

3.4.2.2 Calculation of surface BRF

In the online mode, surface BRF products are produced every 60 minutes. ABI will obtain four sets of images within the 60-minutes window. Depending on the availability of clear-sky observation at the timestamp and BRDF parameters from the offline process, the calculation of surface BRF are led to several different paths over each pixel:

1. When valid clear-sky observation exists,
    a. BRF is retrieved by assuming the Lambertian surface with the latest clear-sky observation as input (algorithm R3);
2. When none valid clear-sky observation exists,
    a. and when BRDF coefficients from offline process exists, BRF is simulated from BRDF coefficients under specific illumination and viewing geometry (algorithm R3);
    b. and when no BRDF coefficients retrieved from the routine offline process, filling value is given.

3.4.2.2.1 R1: Atmospheric correction with BRDF model

When BRDF parameters are available, the directional-hemispheric, hemispheric-directional, hemispheric-hemispheric reflectance could be calculated from the BRDF model. The AOD would be obtained from the AOD product or default value. Then the only unknown in equation (8) is the directional-directional reflectance (BRF). Thus, the surface reflectance could be calculated by inverting equation (8). If the reflectance is out of range (negitave, or greater than 1 for snow pixel, or greater than 0.8 for non-snow pixel), the algorithm will use R2 for reflectance. The IMS snow mask data is used to determine the snow condition. The retrieved surface reflectance is sensitive to BRDF uncertainty. Currently, this prototype ideal subroutine is still under test and supposed to be enabled after fully calibration.

3.4.2.2.2 R2: Prediction from BRDF model

BRF could always be calculated from the BRDF model (1), given BRDF parameters and viewing geometry. Numerically, BRF has the following relationship with BRDF:

$$BRF = BRDF * \pi \qquad (26)$$

However, the retrieved BRDF parameters from the offline mode represent average surface conditions of the compositing time period. Large uncertainties exist when we predict instantaneous surface BRF from the offline BRDF parameters. This prediction is used as back-up method when no clear-sky observation is available.

3.4.2.2.3 R3: Lambertian correction

We assume the surface is Lambertian and obtain a simplified form of equation (8):

$$r = r_0 + \frac{r_s}{1 - r_s \rho} \gamma \qquad (27)$$

where r is TOA reflectance, r_s is surface reflectance, ρ is spherical albedo, r_0 is path reflectance, and γ is transmittance. Given viewing geometry and AOD, ρ, r_0 and γ could be obtained from the LUT. Thus, the surface reflectance could be solved from the following equation:

$$r_s = \frac{r - r_0}{\gamma + (r - r_0)\rho} \qquad (28)$$

3.5 Algorithm Output

The outputs of the LSA algorithm offline mode mainly include the three parameters of the BRDF model for each ABI band (Table 3.11), which will be used as one input of the online mode. The final outputs of the LSA algorithm online mode are instantaneous LSA and BRFs (Table 3.12 and 3.13).

Table 3.11. Outputs of the ABI albedo algorithm offline mode.

Name	Type	Description	Dimension
Ch1 f_iso	float	BRDF isotropic component parameter at Ch1	grid (xsize, ysize)
Ch1 f_vol	float	BRDF volumetric kernel parameter at Ch1	grid (xsize, ysize)
Ch1 f_geo	float	BRDF geometric kernel parameter at Ch1	grid (xsize, ysize)
Ch2 f_iso	float	BRDF isotropic component parameter at Ch2	grid (xsize, ysize)
Ch2 f_vol	float	BRDF volumetric kernel parameter at Ch2	grid (xsize, ysize)
Ch2 f_geo	float	BRDF geometric kernel parameter at Ch2	grid (xsize, ysize)
Ch3 f_iso	float	BRDF isotropic component parameter at Ch3	grid (xsize, ysize)
Ch3 f_vol	float	BRDF volumetric kernel parameter at Ch3	grid (xsize, ysize)
Ch3 f_geo	float	BRDF geometric kernel parameter at Ch3	grid (xsize, ysize)
Ch5 f_iso	float	BRDF isotropic component parameter at Ch5	grid (xsize, ysize)
Ch5 f_vol	float	BRDF volumetric kernel parameter at Ch5	grid (xsize, ysize)

Ch5 f_geo	float	BRDF geometric kernel parameter at Ch5	grid (xsize, ysize)
Ch6 f_iso	float	BRDF isotropic component parameter at Ch6	grid (xsize, ysize)
Ch6 f_vol	float	BRDF volumetric kernel parameter at Ch6	grid (xsize, ysize)
Ch6 f_geo	float	BRDF geometric kernel parameter at Ch6	grid (xsize, ysize)
QF	char	Quality flag for each pixel, indicating the general retrieval quality	grid (xsize, ysize)

Table 3.12. Outputs of the ABI albedo algorithm online mode: LSA

Name	Type	Description	Dimension
Shortwave Albedo	float	Shortwave broadband albedo value at 0.4-3.0 μm	grid (xsize, ysize)
Albedo QF	char	Quality flag for each pixel, indicating the general retrieval quality	grid (xsize, ysize)

Table 3.13. Outputs of the ABI albedo algorithm online mode: BRF

Name	Type	Description	Dimension
Ch1 Ref	float	Derived bidirectional reflectance value at 0.47 μm	grid (xsize, ysize)
Ch2 Ref	float	Derived bidirectional reflectance value at 0.64 μm	grid (xsize, ysize)
Ch3 Ref	float	Derived bidirectional reflectance value at 0.86 μm	grid (xsize, ysize)
Ch5 Ref	float	Derived bidirectional reflectance value at 1.61 μm	grid (xsize, ysize)
Ch6 Ref	float	Derived bidirectional reflectance value at 2.26 μm	grid (xsize, ysize)
Reflectance QF	char	Quality flag for each pixel, indicating the general retrieval quality	grid (xsize, ysize)

The GOES-R ABI LSA and BRF products are generated from multiple paths with various levels of uncertainties. Detailed quality information is critical to the end users. Correspondingly, we also have three groups of Quality Flag (QF). One is for the intermediate BRDF parameter products, the second group is for albedo products, and the third group is for reflectance products. The three groups of QF are defined in Tables 3.14-16.

Table 3.14. QF definition of ABI intermediate BRDF parameter products

Bit	Name	Value
0	Retrieval successful	0: BRDF successfully retrieved 1: Routine algorithm fails
1	Empty	Reserved for future usage
2		
3		
4		
5		
6		
7		

Table 3.15. QF definition of ABI LSA products

Bit	Name	Value
0	Land mask	0:land, 1: water
1	SZA	0:SZA<67, 1: SZA>=67
2	LZA	0:LZA<70, 1: LZA>=70
3	Retrieval path	00:Routine algorithm, 01:Back-up algorithm, 10: Graceful degradation,11: No retrieval
4		
5	Additional info	Used for routine algorithm only 0: valid AOD or COD, 1: no valid AOD or COD,
6	Empty	Reserved for future usage
7		

Table 3.16. QF definition of ABI BRF products

Bit	Name	Value
0	Land mask	0:land, 1: water
1	SZA	0:SZA<67, 1: SZA>=67
2	LZA	0:LZA<70, 1: LZA>=70

3 4	Retrieval path	00:R1, 01:R2, 10: R3,11: at least one band has no retrieval
5 6 7	Empty	Reserved for future usage

Besides the QF info, each file of BRDF parameters, LSA and BRF products also comes with metadata information. The metadata information is given in Tables 3.17-19.

Table 3.17. Attributes or Metadata of ABI intermediate BRDF parameter products

Metadata	Source	Definition
Dimensions	Common	Number of rows/ columns/ bands
FillValue	BRDF_Parameters/ BRDF_QF	"-999.f"/"-128b"
long_name	BRDF_Parameters/ BRDF_QF	"Bidirectional reflectance distribution function parameters"/ "Bidirectional reflectance distribution function quality flag" (0 is successful retrieval; 1 is unsuccessful retrieval)
units	BRDF_Parameters/ BRDF_QF	"1"/ "1" (Dimensionless)
valid_range	BRDF_Parameters/ BRDF_QF	"0.f, 1.f"/ "0b, 1b"
Conventions	Global attribute	"CF-1.5"
summary	Global attribute	"Bidirectional reflectance distribution function parameters that describes the directional properties of reflectivity"
cdm_data_type	Global attribute	"Image"
platform_id	Global attribute	"G16"
orbital_slot	Global attribute	"GOES-East"
instrument_type	Global attribute	"GOES-R Series Advanced Baseline Imager"
spatial_resolution	Global attribute	"2km at nadir"

scene_id	Global attribute	“Full Disk”

Table 3.18. Attributes or Metadata of ABI LSA products

Metadata	Source	Definition
Date	common	Beginning and end dates of the product
Time	common	Beginning and end times of the product
Dimension	common	Number of rows, number of columns
Product Name	common	The ABI land surface albedo product
Satellite	common	GOES-R satellite name
Instrument	common	ABI
Version	common	Product version number
Filling Value	LSA	Value representing no data produced
Valid Range	LSA	Valid range of albedo values, 0-1
MeanAlb	LSA[1]	Average Albedo value
StdAlb	LSA[1]	Standard deviation of Albedo
MaxAlb	LSA[1]	Maximum Albedo value
MinAlb	LSA[1]	Minimum Albedo value
AlbPercHighQuality	LSA QC[2]	Number of High Quality Retrieval
AlbPercMedQuality	LSA QC[2]	Number of medium Quality Retrieval
AlbPercInvalid	LSA QC[2]	Number of Invalid Retrieval
AlbPercLandValid	LSA QC[2]	Number of valid land pixels
AlbPercWaterValid	LSA QC[2]	Number of valid water pixels
AlbPercAODValid	LSA QC[2]	Number of pixels with valid AOD or COD
AlbPercAODInvalid	LSA QC[2]	Number of pixels with invalid AOD or COD
AlbPercSZAFav	LSA QC[2]	Number of pixels with Favorable SZA
AlbPercVZAFav	LSA QC[2]	Number of pixels with very large SZA
AlbPercSZALarge	LSA QC[2]	Number of pixels with Favorable VZA
AlbPercVZALarge	LSA QC[2]	Number of pixels with very large VZA

Table 3.19. Attributes or Metadata of ABI BRF products

Metadata	Source	Definition

Date	common	Beginning and end dates of the product
Time	common	Beginning and end times of the product
Dimension	common	Number of rows, number of columns
Product Name	common	The ABI land surface reflectance product
Satellite	common	GOES-R satellite name
Instrument	common	ABI
Version	common	Product version number
Filling Value	BRF	Value representing no data produced
Valid Range	BRF	Valid range of reflectance values, 0-2
MaxRef1	BRF[1]	Maximum Reflectance Band1
MinRef1	BRF[1]	Minimum Reflectance Band1
MeanRef1	BRF[1]	Average Reflectance Band1
StdRef1	BRF[1]	Standard deviation of Reflectance Band 1
MaxRef2	BRF[1]	Maximum Reflectance Band2
MinRef2	BRF[1]	Minimum Reflectance Band2
MeanRef2	BRF[1]	Average Reflectance Band2
StdRef2	BRF[1]	Standard deviation of Reflectance Band 2
MaxRef3	BRF[1]	Maximum Reflectance Band3
MinRef3	BRF[1]	Minimum Reflectance Band3
MeanRef3	BRF[1]	Average Reflectance Band3
StdRef3	BRF[1]	Standard deviation of Reflectance Band 3
MaxRef5	BRF[1]	Maximum Reflectance Band5
MinRef5	BRF[1]	Minimum Reflectance Band5
MeanRef5	BRF[1]	Average Reflectance Band5
StdRef5	BRF[1]	Standard deviation of Reflectance Band 5
MaxRef6	BRF[1]	Statistics from Ch6_Ref
MinRef6	BRF[1]	Statistics from Ch6_Ref
MeanRef6	BRF[1]	Statistics from Ch6_Ref
StdRef6	BRF[1]	Statistics from Ch6_Ref
RefPercHighQuality	BRF QC[2]	Statistics from Ref_QF “Bit 3-4: 00”
RefPercMedQuality	BRF QC[2]	Statistics from Ref_QF “Bit 3-4: 01 and 10”

RefPercInvalid	BRF QC[2]	Statistics from Ref_QF “Bit 3-4: 11”
RefPercLandValid	BRF QC[2]	Statistics from Ref_QF "Bit 0: 0 & Bit 3-4: not equal to 11”
RefPercWaterValid	BRF QC[2]	Statistics from Ref_QF "Bit 0: 1 & Bit 3-4: not equal to 11”
RefPercSZAFav	BRF QC[2]	Statistics from Ref_QF “Bit 1: 0”
RefPercVZAFav	BRF QC[2]	Statistics from Ref_QF “Bit 1: 1”
RefPercSZALarge	BRF QC[2]	Statistics from Ref_QF “Bit 2: 0”
RefPercVZALarge	BRF QC[2]	Statistics from Ref_QF “Bit 2: 1”

*Note:

1. The statistics items are calculated on the pixels with valid retrievals (i.e., $0 \leq LSA \leq 1, 0 \leq BRF \leq 2$);

2. The Percents items are calculated from the on-earth-pixels, i.e, excluding the space pixels in both the numerator and the denominator. The space pixel mask is included in L1B navigation data.

3.6 GOES-17 Loop Heat Pipe Anomaly Mitigation

Post-launch testing of GOES-17 has discovered an issue with the instruments’ cooling system in the loop heat pipe (LHP) subsystem. The issue has caused inadequate cooling of the infrared channels, leading to partial loss of long-wave imagery data. Considering the imagery data in shortwave window is still available over the daytime, the albedo algorithm does not suffer from direct data missing, but with consequent risk from using the cloud mask data which needs the thermal bands as input.

A granule-level quality flag, as a 64 bit integer called "granule_level_quality_flag", has been inherited from the cloud mask product to reveal the LHP effect. In the cloud mask algorithm, each required IR channel has a specific focal plane temperature (FPT) threshold that is determined, which would test the maximum FPT from the channel L1B file against this threshold. If the FTP exceeds the corresponding threshold, the channel is turned off. The "granule_level_quality_flag" has a value 0 for good and bits that are set for things like channel degradation, missing dynamic ancillary input or complete failure. This variable can alert the algorithm if the cloud mask is degraded by testing the specific bit for channel degradation and users could keep cautious when use that granule.

4 TEST DATA SETS AND OUTPUTS

The algorithm was tested using simulation data, AHI data, and ABI data. Both LSA products and BRF products have been validated.

4.1 Sample Output

Figure 4.1 ~ 4.3 show sample images of online albedo, albedo quality flag, reflectance, and reflectance quality flag, and the corresponding BRDF of GOES-16. Figure 4.4 ~ 4.6 show sample images of simultaneous images of GOES-17. The sample data was produced in the Framework v2.0.

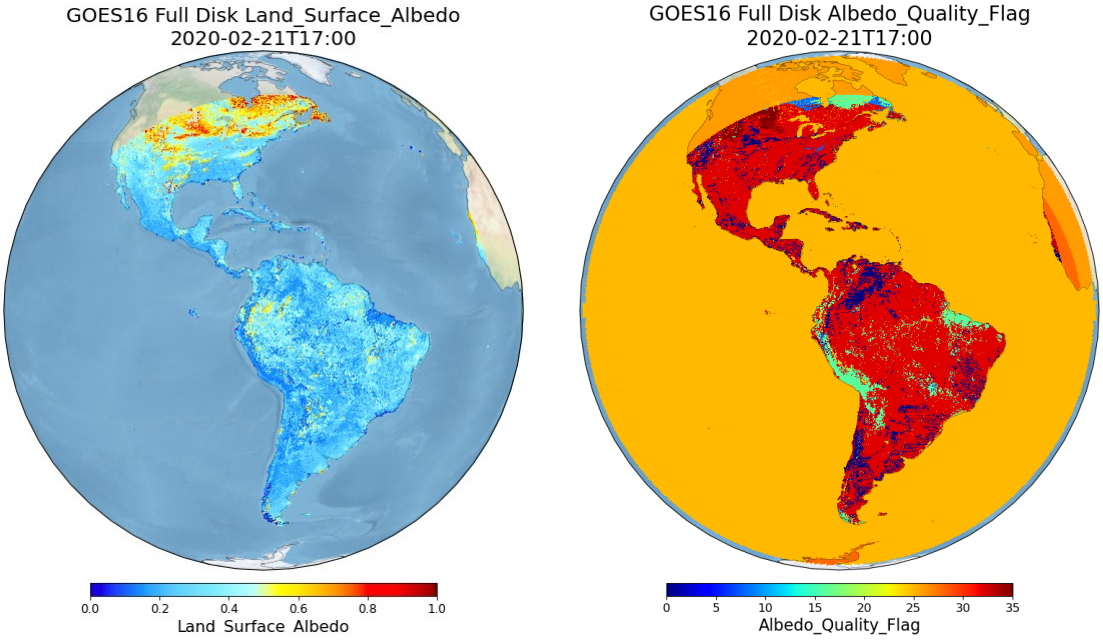

(a) (b)

Figure 4.1 Plots of GOES16 Full Disk Albedo (a) and its quality flag (b) on Feb 21, 2020 at 17:00 UTC.

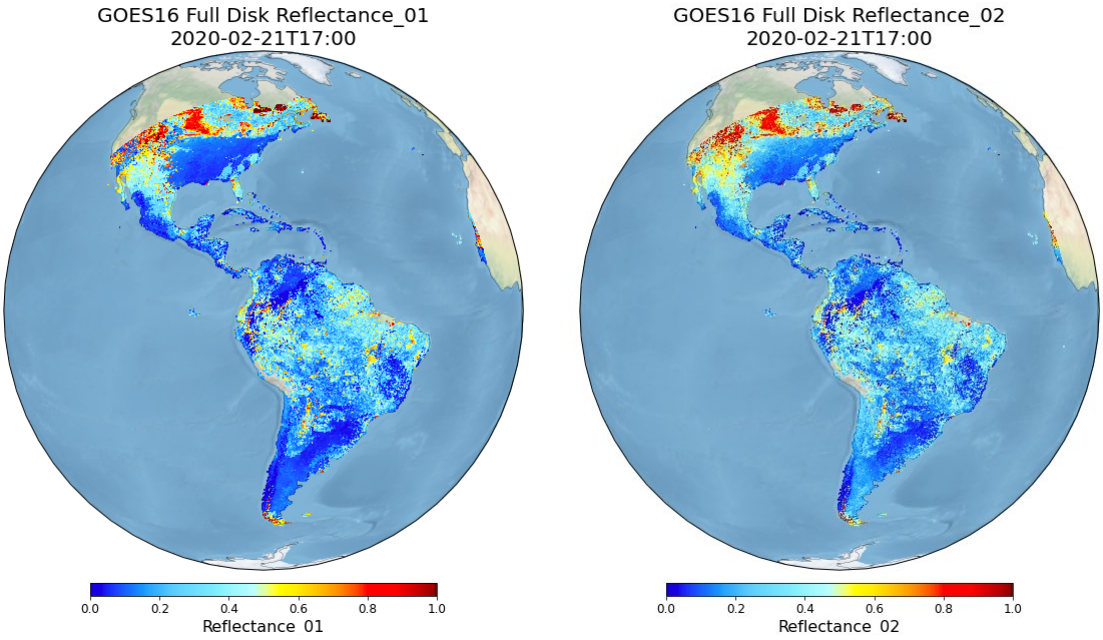

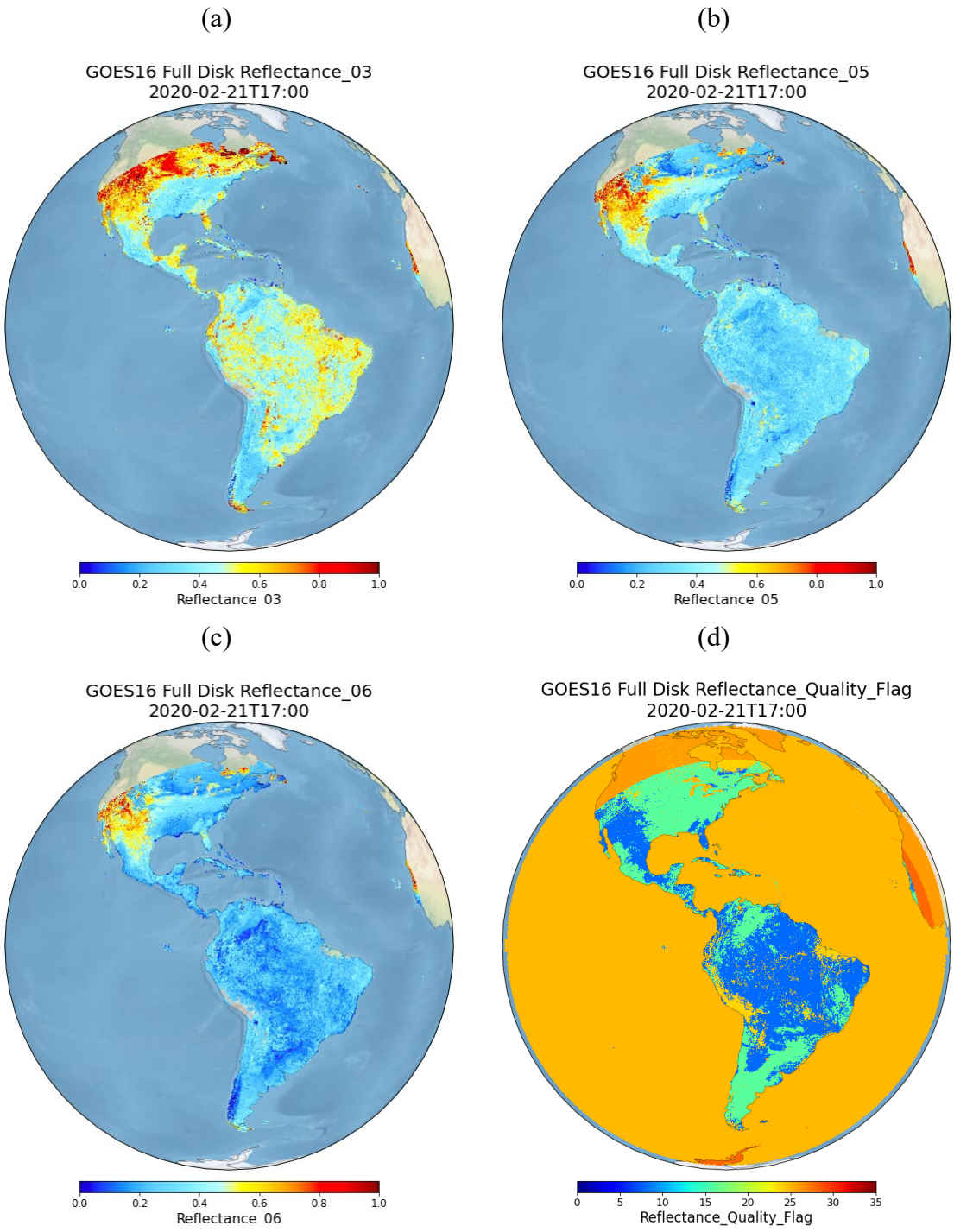

Figure 4.2 Plots of GOES16 Full Disk Reflectance at band 1,2,3,5,6 (a~e) and the quality flag (f) on Feb 21, 2020 at 17:00 UTC.

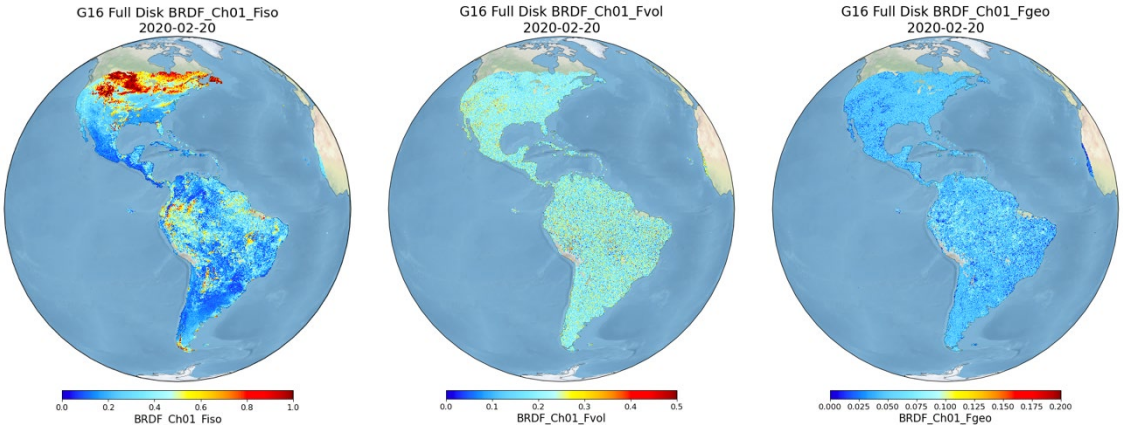
G16 Full Disk BRDF_Ch01_Fiso
2020-02-20
0.0 0.2 0.4 0.6 0.8 1.0
BRDF_Ch01_Fiso
G16 Full Disk BRDF_Ch01_Fvol
2020-02-20
0.0 0.1 0.2 0.3 0.4 0.5
BRDF_Ch01_Fvol
G16 Full Disk BRDF_Ch01_Fgeo
2020-02-20
0.000 0.025 0.050 0.075 0.100 0.125 0.150 0.175 0.200
BRDF_Ch01_Fgeo

(a) (b) (c)

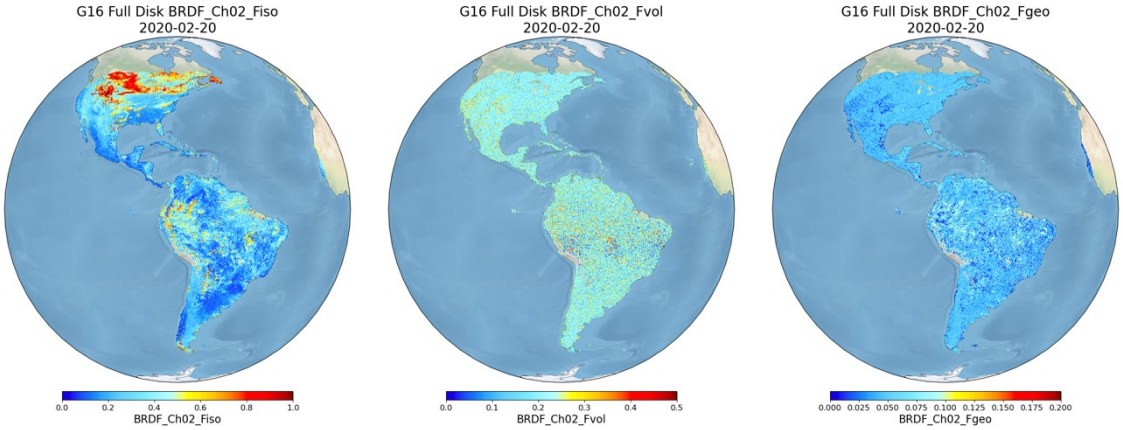
G16 Full Disk BRDF_Ch02_Fiso
2020-02-20
0.0 0.2 0.4 0.6 0.8 1.0
BRDF_Ch02_Fiso
G16 Full Disk BRDF_Ch02_Fvol
2020-02-20
0.0 0.1 0.2 0.3 0.4 0.5
BRDF_Ch02_Fvol
G16 Full Disk BRDF_Ch02_Fgeo
2020-02-20
0.000 0.025 0.050 0.075 0.100 0.125 0.150 0.175 0.200
BRDF_Ch02_Fgeo

(d) (e) (f)

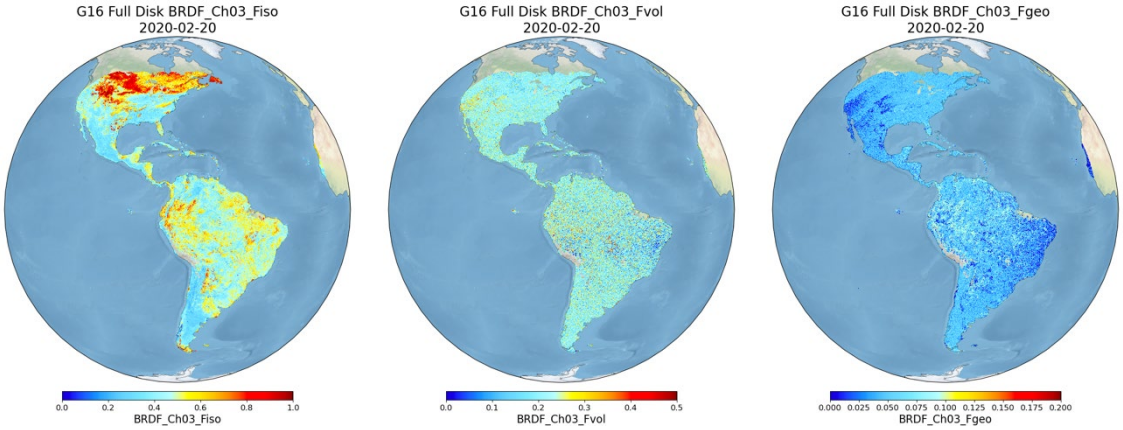
G16 Full Disk BRDF_Ch03_Fiso
2020-02-20
0.0 0.2 0.4 0.6 0.8 1.0
BRDF_Ch03_Fiso
G16 Full Disk BRDF_Ch03_Fvol
2020-02-20
0.0 0.1 0.2 0.3 0.4 0.5
BRDF_Ch03_Fvol
G16 Full Disk BRDF_Ch03_Fgeo
2020-02-20
0.000 0.025 0.050 0.075 0.100 0.125 0.150 0.175 0.200
BRDF_Ch03_Fgeo

(g) (h) (i)

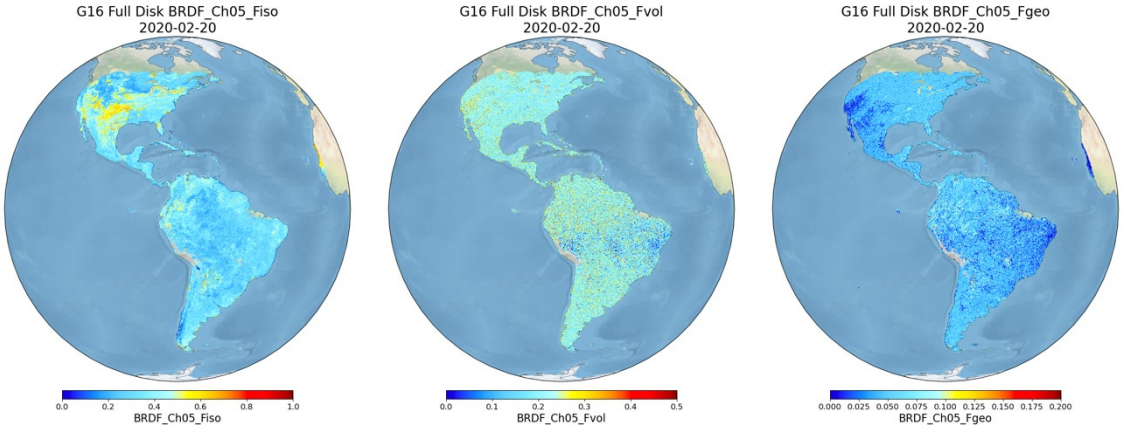

(j) (k) (l)

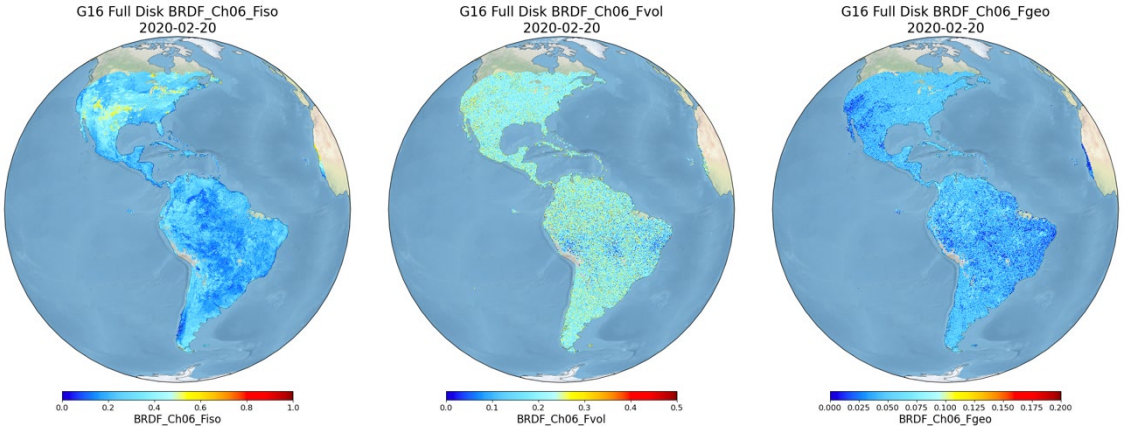

(m) (n) (o)

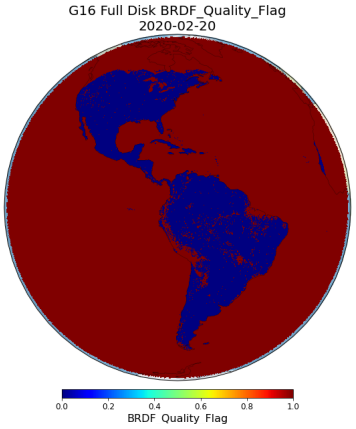

(p)

Figure 4.3 Plots of GOES16 Full Disk BRDF at band 1,2,3,5,6 (a~e) and the quality flag (f) from Feb 20, 2020.

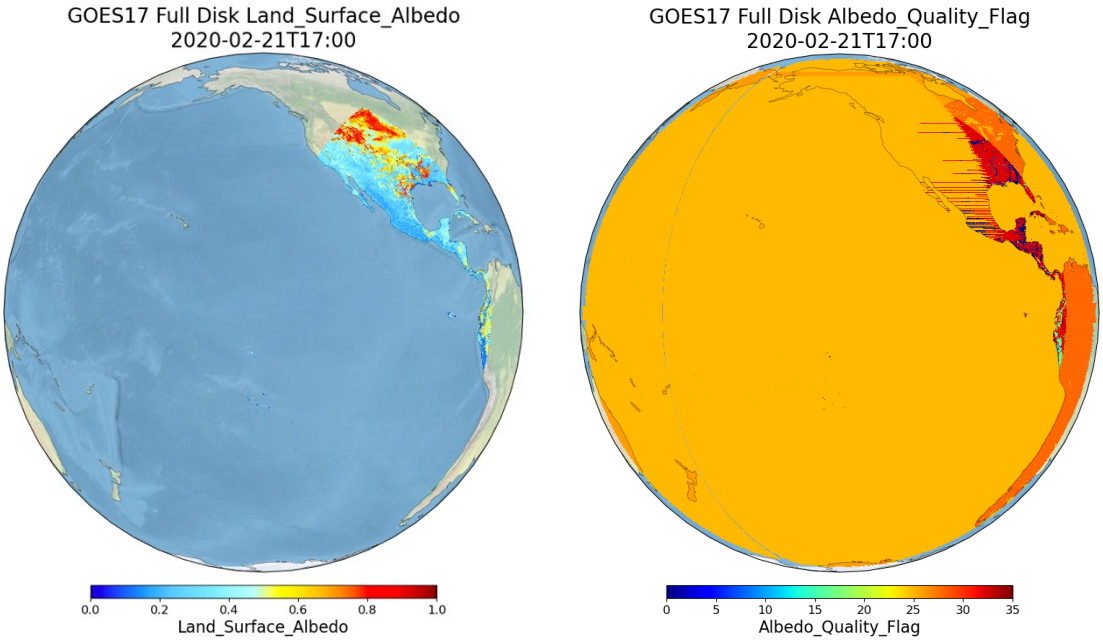

(a) (b)

Figure 4.4 Plots of GOES17 Full Disk Albedo (a) and its quality flag (b) on Feb 21, 2020 at 17:00 UTC.

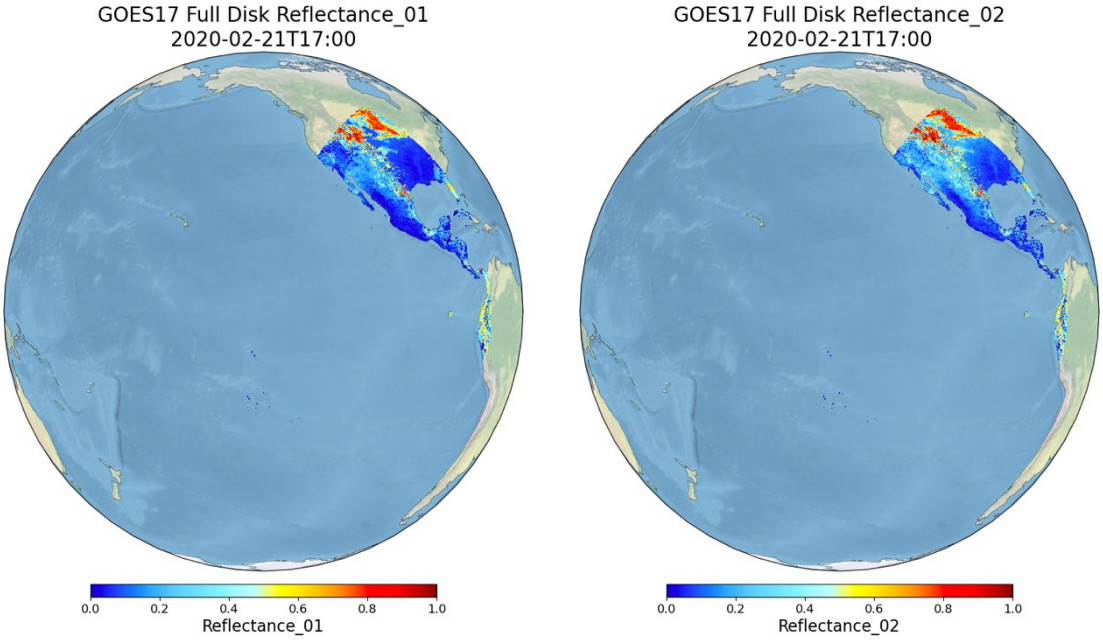

(a) (b)

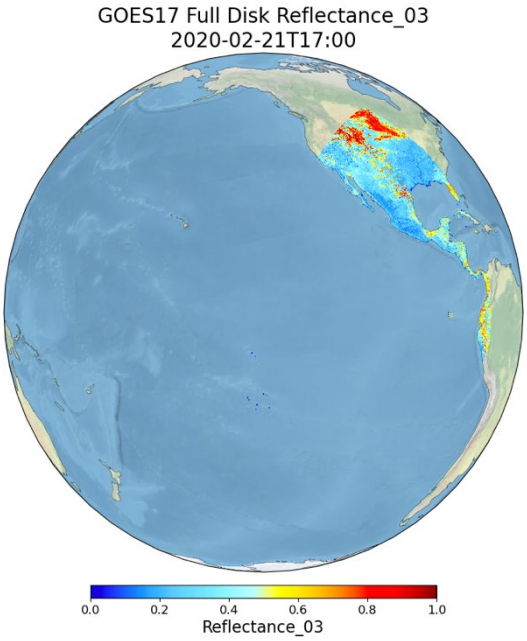

(c)

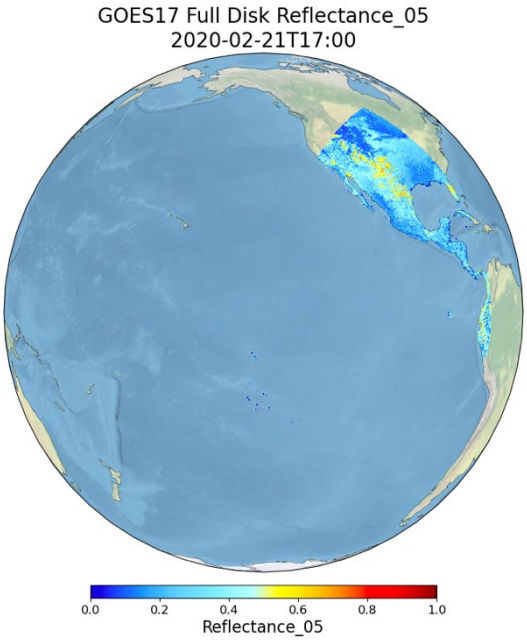

(d)

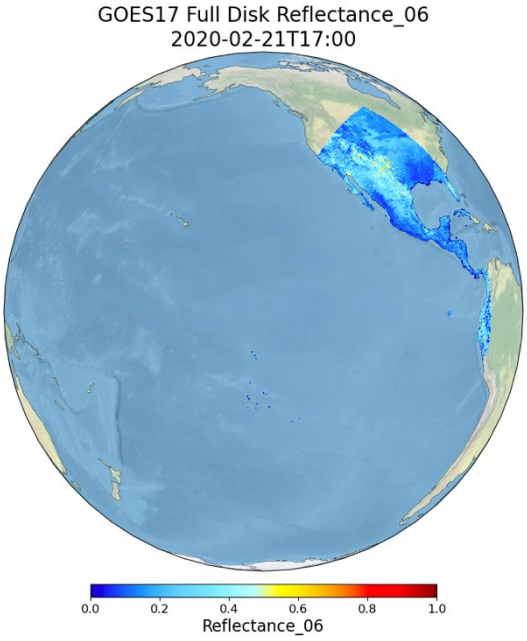

(e)

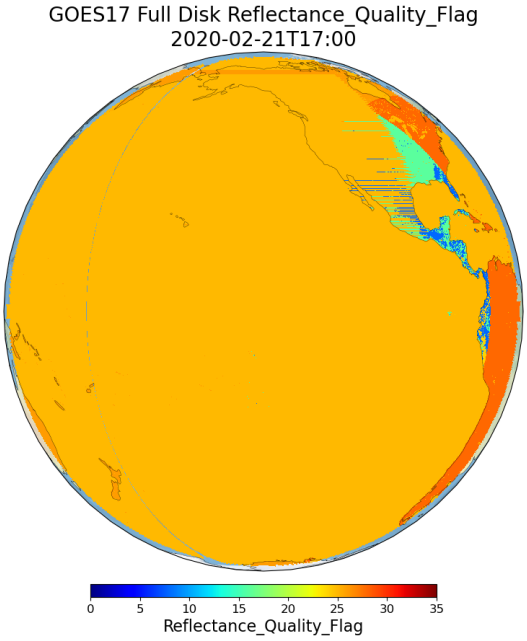

(f)

Figure 4.5 Plots of GOES17 Full Disk Reflectance at band 1,2,3,5,6 (a~e) and the quality flag (f) on Feb 21, 2020 at 17:00 UTC.

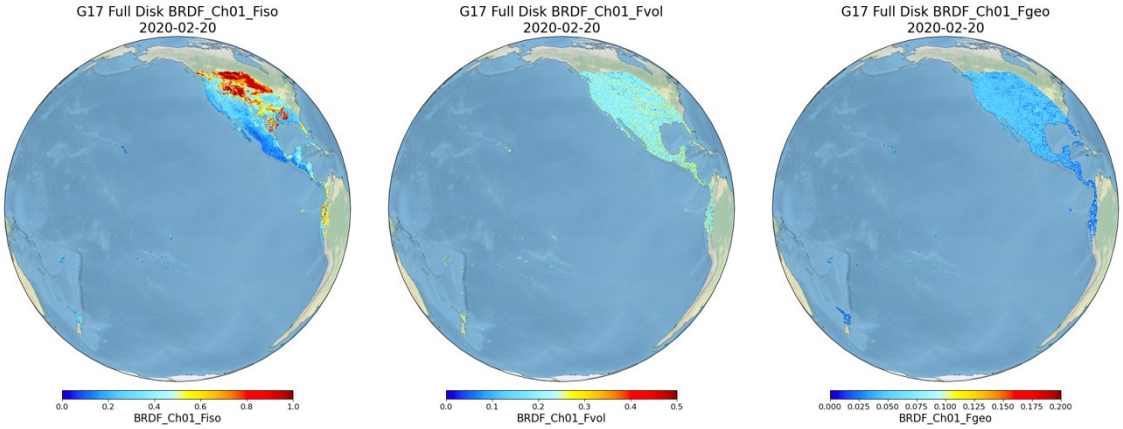
G17 Full Disk BRDF_Ch01_Fiso
2020-02-20
0.0 0.2 0.4 0.6 0.8 1.0
BRDF_Ch01_Fiso
G17 Full Disk BRDF_Ch01_Fvol
2020-02-20
0.0 0.1 0.2 0.3 0.4 0.5
BRDF_Ch01_Fvol
G17 Full Disk BRDF_Ch01_Fgeo
2020-02-20
0.000 0.025 0.050 0.075 0.100 0.125 0.150 0.175 0.200
BRDF_Ch01_Fgeo

(a) (b) (c)

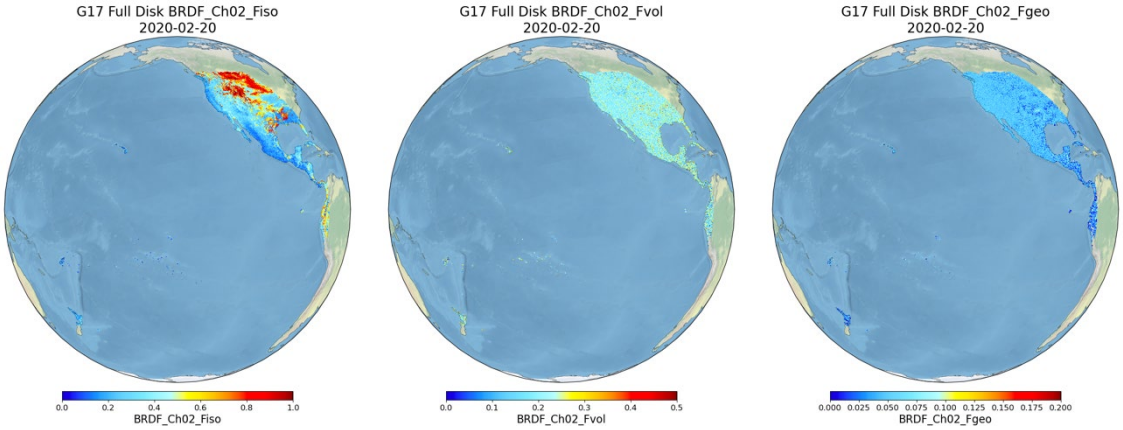
G17 Full Disk BRDF_Ch02_Fiso
2020-02-20
0.0 0.2 0.4 0.6 0.8 1.0
BRDF_Ch02_Fiso
G17 Full Disk BRDF_Ch02_Fvol
2020-02-20
0.0 0.1 0.2 0.3 0.4 0.5
BRDF_Ch02_Fvol
G17 Full Disk BRDF_Ch02_Fgeo
2020-02-20
0.000 0.025 0.050 0.075 0.100 0.125 0.150 0.175 0.200
BRDF_Ch02_Fgeo

(d) (e) (f)

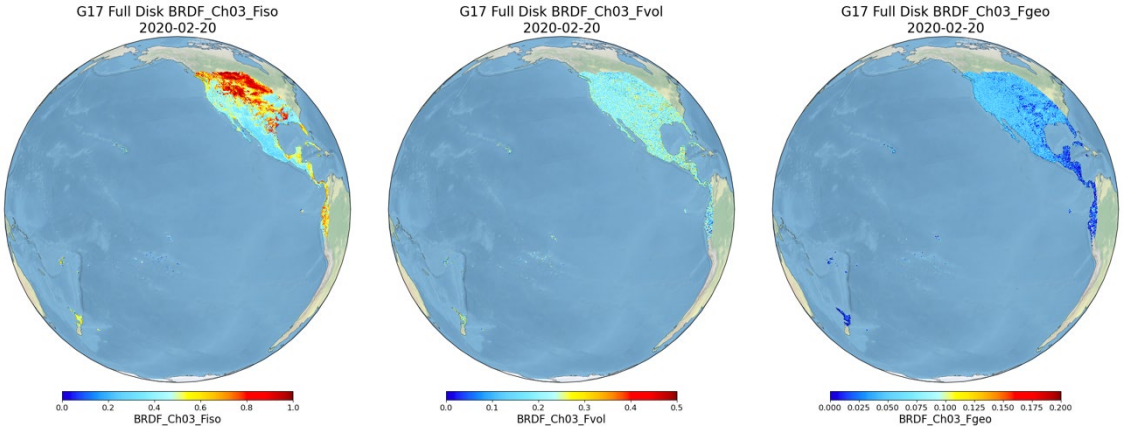
G17 Full Disk BRDF_Ch03_Fiso
2020-02-20
0.0 0.2 0.4 0.6 0.8 1.0
BRDF_Ch03_Fiso
G17 Full Disk BRDF_Ch03_Fvol
2020-02-20
0.0 0.1 0.2 0.3 0.4 0.5
BRDF_Ch03_Fvol
G17 Full Disk BRDF_Ch03_Fgeo
2020-02-20
0.000 0.025 0.050 0.075 0.100 0.125 0.150 0.175 0.200
BRDF_Ch03_Fgeo

(g) (h) (i)

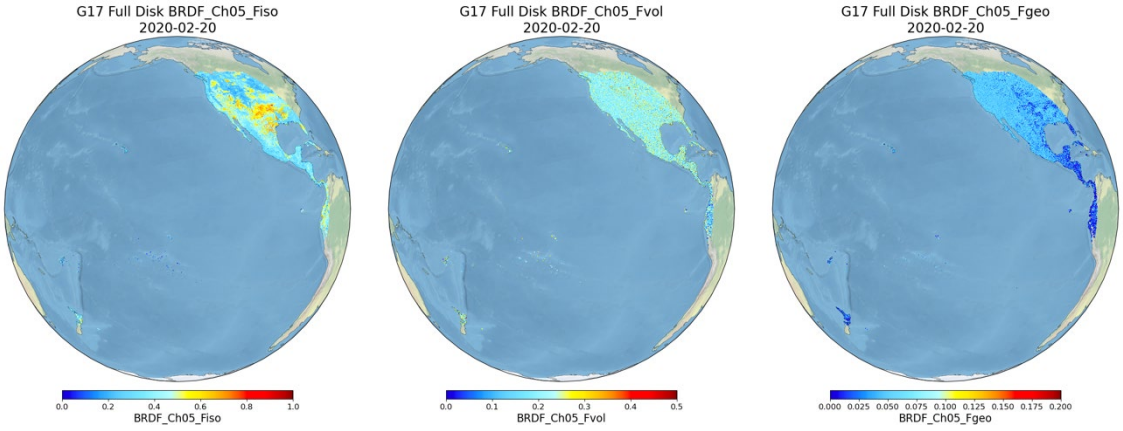

(j) (k) (l)

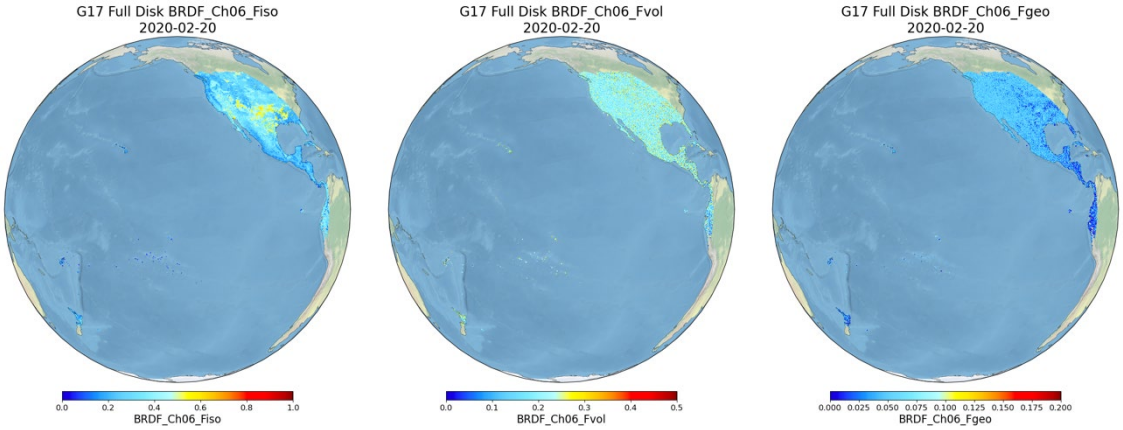

(m) (n) (o)

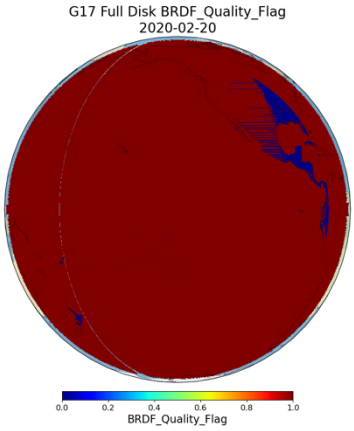

(p)

Figure 4.6 Plots of GOES17 Full Disk BRDF at band 1,2,3,5,6 (a~e) and the quality flag (f) from Feb 20, 2020.

4.2 Validation using simulation data

4.2.1 Input Data

One characteristic of the ABI LSA algorithm is that it takes advantage of two features of ABI measurements -- high temporal refreshing rates and multi-spectral configuration -- to achieve the goal of retrieving atmospheric conditions and surface BRDF parameters simultaneously. MODIS has similar spectral configuration (seven bands for the land application) to ABI. However, MODIS is a polar-orbiting sensor and maps the Earth surface only twice in most cases even if we combine both Terra and Aqua satellites. Table 4.1 lists the visible and near infrared bands of the MODIS and ABI. We firstly carried out the simulation of radiative transfer and use simulated ABI data to test the LSA algorithm.

Table 4.1. Comparison of MODIS and ABI reflective bands.

Sensor	Temporal resolution	Channel No.	Wavelength Center (μm)	Bandwidth (μm)
ABI	15min	1	0.47	0.45 – 0.49
		2	0.64	0.59 – 0.69
		3	0.86	0.85 – 0.88
		5	1.61	1.58 – 1.64
		6	2.26	2.23 – 2.28
MODIS	Polar-orbitting	1	0.646	0.62-0.67
		2	0.857	0.84-0.88
		3	0.466	0.46-0.48
		4	0.554	0.55-0.57
		5	1.242	1.23-1.25
		6	1.629	1.63-1.65
		7	2.114	2.11-2.16

4.2.1.1 **Simulated Data**

Since none of existing satellite sensors can provide proxy data with both the high temporal resolution and multiple-channels as ABI data, simulation will be the only way to test our algorithm's ability to handle ABI data before GOES-R is launched. We use Qin et al.

(2001)'s formulation of atmospheric radiative transfer to simulate TOA signals and assure the simulated TOA signals have the following properties:

- Use the ABI band configuration and band response functions.
- Bear the realistic observing geometry and refreshing rate of ABI.
- Consider the couple between the atmosphere and surface BRFs.

In order to simulate the signals received by the spaceborne sensors, both the surface properties and atmospheric parameters are needed in addition to the sensor response functions. We use the BRDF parameters from the MODIS albedo products as the input of surface properties. The AOD data come from the field measurements at SURFRAD sites as the atmospheric conditions. Similar to the solar radiation, AOD is also measured every 3 minutes using visible Multi-Filter Rotating Shadowband Radiometers (MFRSR). SURFRAD AOD measurements include five bands (415.0, 501.6, 613.5, 671.7 and 867.5nm). However, the 6S simulation requires the AOD input at 550nm. We calculate this value using the Angstrom Equation:

$$\tau_\lambda = \beta\lambda^{-\alpha}$$

where λ is the wavelength, τ_λ is the AOD at λ. α and β are coefficients, which are obtained through the linear regression if AOD measurements at three bands are valid. An example of such time series of AOD at 550nm is given in Figure 4.7.

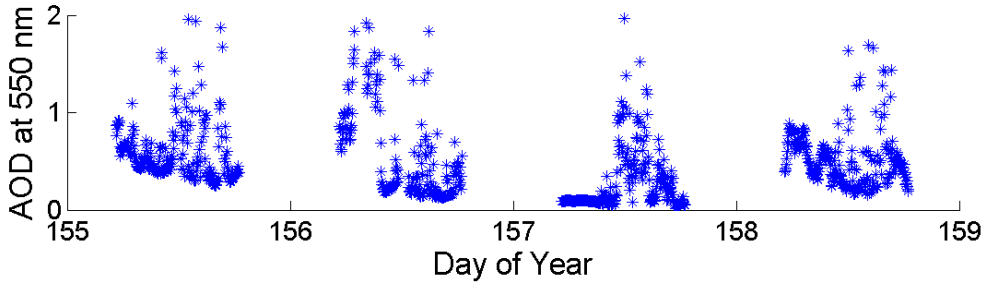

Figure 4.7 An example input of AOD time series at the Bondville site. The AODs at 550nm are calculated from AODs at other bands using the Angstrom Equation.

4.2.1.2 **MODIS Data**

We carried out two types of validation activities using MODIS as proxy data. First, we extracted the point data over a couple of sites, SURFRAD, AmeriFlux and GC-Net sites for the whole year of 2005 and directly compare our retrievals with field measurements. We also generated a time series of ten days' MODIS data as proxy data to test the operational ability of the LSA algorithm over 2D images. MODIS is a polar-orbiting sensor. The L1B MODIS swath cannot be directly used to stack the time series because each of these swaths has different spatial coverage. We have to project all the MODIS L1B swath data to a common map projection and stack them as time series data.

4.2.2 Ground Measurements

4.2.2.1 **Measurement of albedo**

Albedo measurements over SURFRAD, AmeriFlux and GC-Net networks are used in our validation (Table 4.2-4). Albedo is calculated as the ratio of outgoing and incoming solar irradiance. Incoming and outgoing shortwave radiation is measured every 3 minutes at SURFRAD sites using the Eppley Precision Spectral Pyranometers (PSP), which are calibrated annually. The averages of albedo over 30 minutes are used to compare with instantaneous albedo retrieved by our algorithm to mitigate the mismatch.

As many of the AmeriFlux sites do not have measurements on both shortwave upward and downward radiation, the visible radiation measurements are used in this study. Unlike the SURFRAD sites, the AmeriFlux sites refresh their measurements only every half an hour, so that a one-hour temporal window is used to calculate the "ground truth" blue-sky albedo similar to the SURFRAD data.

Ground radiation measurements over Greenland are regularly collected by the Greenland Climate Network (GC-Net). This data set provides unique and extensive observations which can help verify the validity of this proposed algorithm over snow-covered surfaces. Shortwave upward and downward radiation is observed on an hourly basis. The "ground truth" blue-sky albedo is calculated based on that. Thirteen sites were chosen in this study according to data availability and data quality during the year of 2003.

Table 4.2. Information of SURFRAD Stations

Site No.	Site Location	Latitude	Longitude	Surface types
1	Bondville, IL	40.05	-88.37	Crop
2	Desert Rock, NV	36.63	-116.02	Open shrub
3	Fort Peck, MT	48.31	-105.10	Grass
4	Goodwin Creek, MS	34.25	-89.87	Deciduous Forest
5	Pennsylvania State University, PA	40.72	-77.93	Mixed Forest
6	Sioux Falls, SD	43.73	-96.62	Forest

Table 4.3. Information of AmeriFlux Stations

Site No.	Site Location	Latitude	Longitude
1	Fort Peck	48.31	-105.10
2	Fermi(Prairie)	41.84	-88.24

3	Mead(Irrigated)	41.17	-96.48
4	Mead(Rain fed)	41.18	-96.44

Table 4.4. Information of GC-Net Stations

Site Name	Location	Site Name	Location
Swiss Camp	69.5732N, 49.2952W	CP1	69.8819N, 46.9736W
JAR1	69.4981N, 49.6816W	NASA-U	73.8333N, 49.4953W
JAR3	69.3954N, 50.3104W	GITS	77.1433N, 61.0950W
Summit	72.5794N, 38.5042W	Tunu-N	78.0168N, 33.9939W
Saddle	66.0006N, 44.5014W	DYE-2	66.4810, 46.2800W
NASA-SE	66.4797N, 42.5002W	NASA-E	75.0000N, 29.9997W
NGRIP	75.0998N, 42.3326W		

4.2.2.2 **Surrogate of surface reflectance**

Due to the limited spatial representation of ground measurements, it is always difficult to validate satellite pixel-based surface albedo estimations solely by comparing with ground measured data, especially when the pixel is not quite homogeneous. Using other satellite-derived data sources can help verify the algorithm estimations. Based on the ancillary information on aerosol and water vapor from the Aerosol Robotic Network (AERONET) sites, a set of surface albedo and reflectance data is retrieved through an independent atmospheric correction with the Ross-Li BRDF kernel models using TOA data from MODIS observations (Wang et al. 2009). MODASRVN data products from 2000 onwards are stored with the AERONET site in the center of the image covering 50 × 50 km2 at 1 km resolution.

According to the location, land cover type, and MODASRVN data availability from the AERONET sites, sixteen sites were chosen in this study for the validation of the estimated surface reflectance (Table 4.5). Similar to the ground measurement section, data for the year of 2005 for MODASRVN and MODIS level 1B TOA observations were collected and processed.

Table 4.5. MODASRVN – AERONET site information

Site Name	Location	Land Cover	Site Name	Location	Land Cover
Bondville	40.053N, 88.372W	Crop	Mexico City	19.334N, 99.182W	Urban

GSFC	38.993N, 76.840W	Forest & Urban	Rimrock	46.487N, 116.990W	Grass
Missoula	46.917N, 114.080W	Grass & Urban	MD Science Center	39.283N, 76.617W	Urban
SERC	38.883N, 76.500W	Forest & Wetland	KONZAEDC	39.102N, 96.610W	Grass
CARTEL	45.379N, 71.931W	Grass & Urban	BSRNBAO Boulder	40.045N, 105.010W	Grass
Bratts Lake	50.280N, 104.700W	Crop	Railroad Valley	38.504N, 115.960W	Grass
Sioux Falls	43.736N, 96.626W	Grass	Frenso	36.782N, 119.770W	Urban
Egbert	44.226N, 79.750W	Crop	Halifax	44.638N, 63.594W	Urban

4.2.3 Validation Results

4.2.3.1 **Output from Simulated Data**

More validation work using simulated ABI data is ongoing. Preliminary results show our retrieval could capture the BRDF distribution well under a variety of atmospheric and surface settings. One example is given in Figure 4.8. Although the two BRDF data sets come from different empirical models, they have similar reflectance distribution shapes. However, due to the feature of the BRDF model we use in the albedo algorithm, a hot-spot effect is noticeable in our retrieved BRDF distribution.

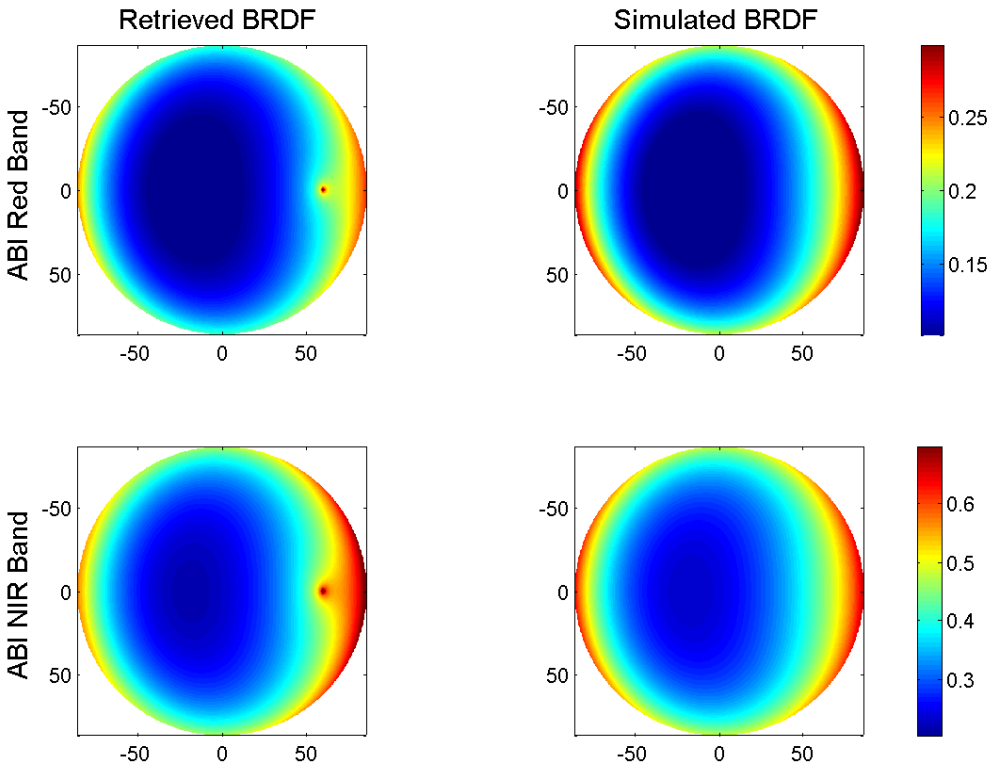

Figure 4.8 The retrieved BRDF and the actual BRDF used in the simulation at ABI red and near infrared bands.

4.2.4 Output from MODIS Data

The LSA algorithm was carried out on these time series of images to generate albedo maps at each observation time. The retrieved blacksky albedo on May 1st, 2005 around 48.3˚N, 102.8˚W is shown in Figure 4.9. The MODIS blacksky albedo for the same time and location is also shown. Our estimation captures a similar spatial pattern to MODIS data but has slight underestimation (Figure 4.10).

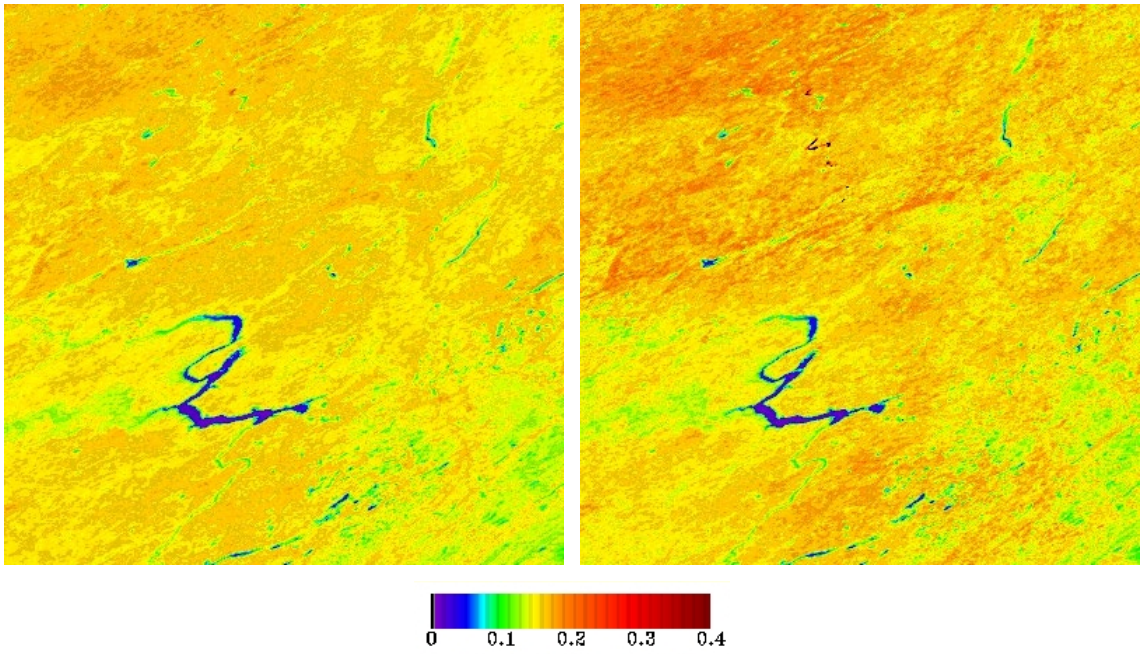

a) Estimated Black-sky Albedo b) MODIS Black-sky Albedo

Figure 4.9 The black-sky albedo maps on May 1st, 2005 around 48.3˚N, 102.8˚W.

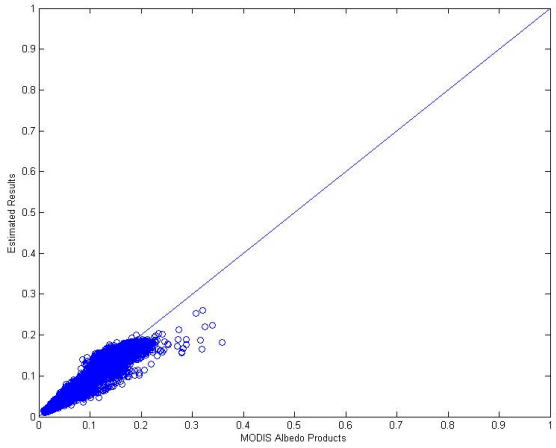

Figure 4.10 Comparison between our retrieved albedo and MODIS albedo.

4.2.5 Validation results of albedo

The direct validation results of our retrieved albedo values over three networks are shown in time series (Figure 4.11). Generally, the retrieved albedo values match well with field measurements. For the non-snow cases (Desert Rock and Goodwin Creek), the Root Mean Square Errors (RMSE) are quite small, although the R^2 values are rather low due to the small range of albedo variations. The undetected clouds may be the main cause of albedo overestimation in Desert Rock. At Goodwin Creek, both our estimations and MODIS products are slightly lower than field measurements. This may come from the inaccurate

representations of aerosol types. Both our retrievals and MODIS albedo data can reasonably represent the seasonal snow albedo over Bondville, Fort Peck and Sioux Falls. Our retrieval algorithm requires shorter compositing window, which makes it possible to better capture the rapid snowfall/melting processes when ABI data are available.

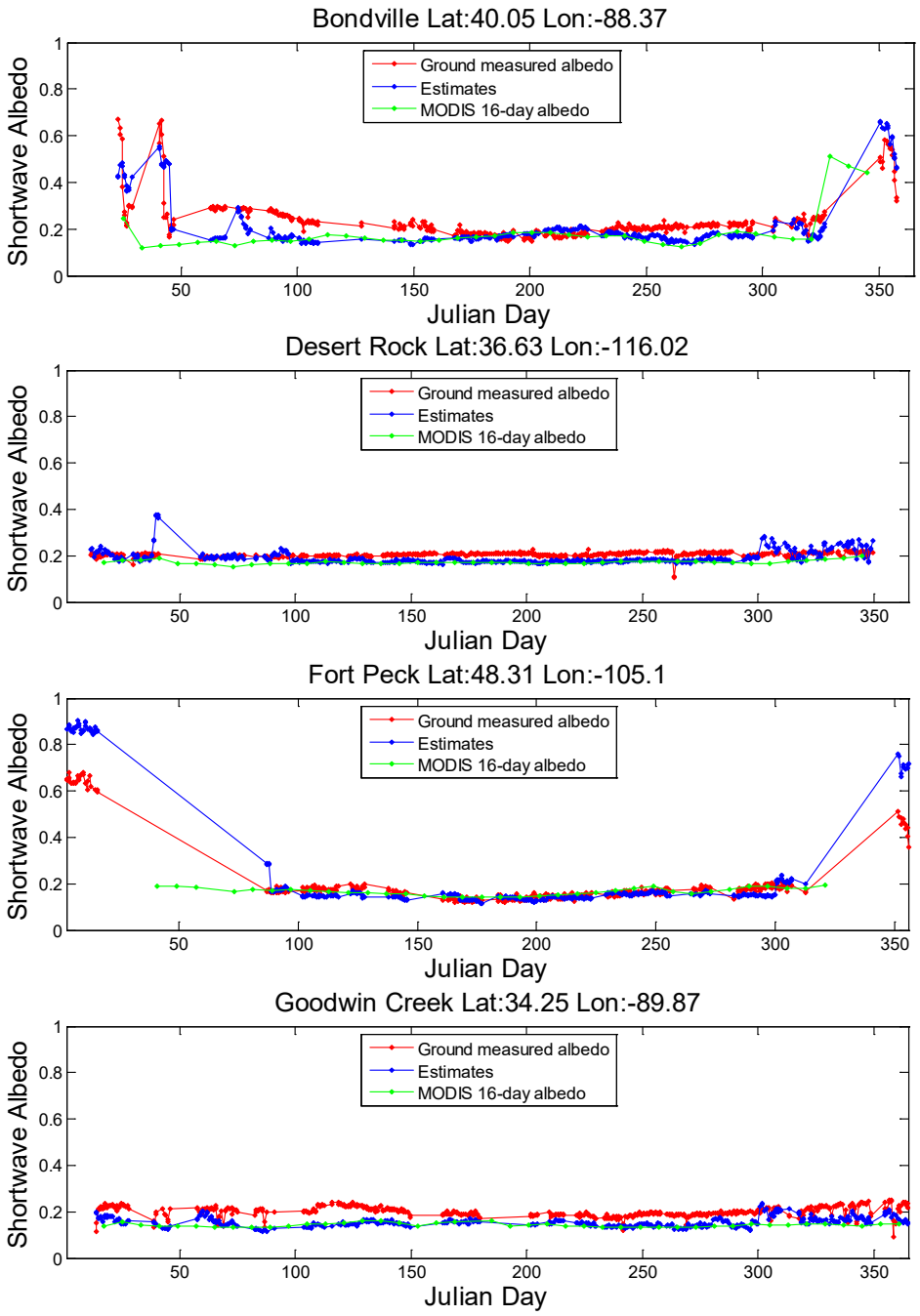

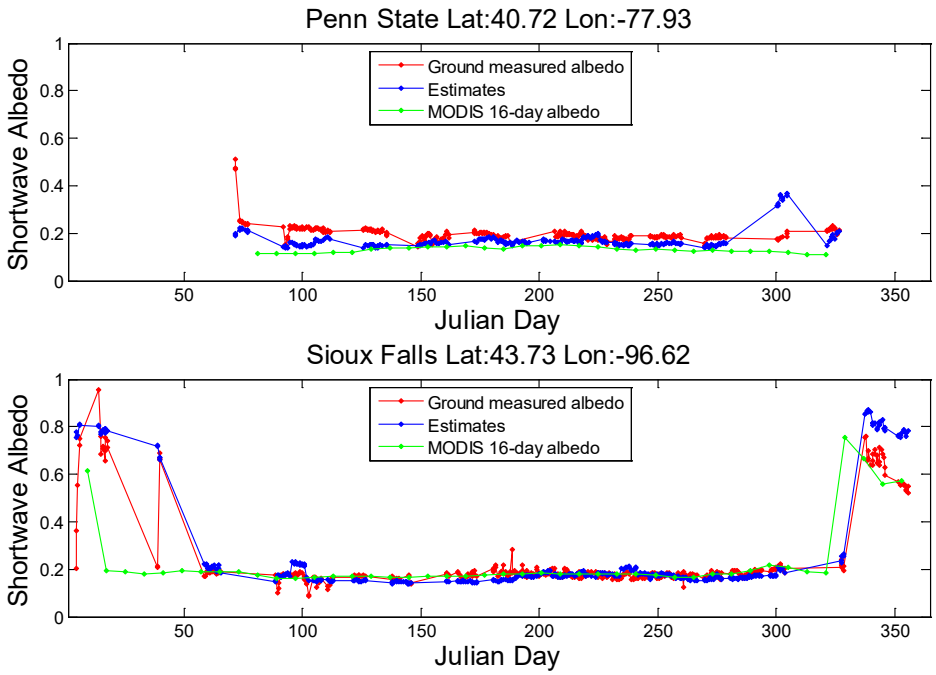

Figure 4.11 Verification of time series shortwave albedo from MODIS observations in 2005 over six SURFRAD sites (blue cross: ground measured shortwave albedo; red cross: estimated albedo from MODIS observations; black cross: MODIS 16-day albedo product).

Table 4.6. Statistics of the retrieved values from this study and MODIS albedo products with comparison to ground measurements over SURFRAD sites

	Bias	STD	RMSE	R^2
Bondville	0.003	0.065	0.071	0.625
Desert Rock	0.014	0.029	0.033	0.006
Fort Peck	-0.016	0.075	0.077	0.969
Goodwin Creek	0.046	0.026	0.053	0.051
Penn State	0.029	0.049	0.056	0.007
Sioux Falls	-0.016	0.072	0.074	0.907
All sites	0.014	0.060	0.062	0.821
All sites from MODIS	0.041	0.055	0.068	0.654

The validation results at four AmeriFlux sites are shown in Figures 4.12. The results shown here are visible albedo because only irradiances in the visible spectrum are measured at these sites. Similar to the results at SURFRAD, our algorithm can capture the annual curves of albedo, but produces larger errors for rapidly changing surfaces. Furthermore, the

MODIS albedo products have several gaps when snow is found over some sites or simply provide snow-free albedo estimations if either there are not enough observations for retrieving or only data with low accuracy can be obtained.

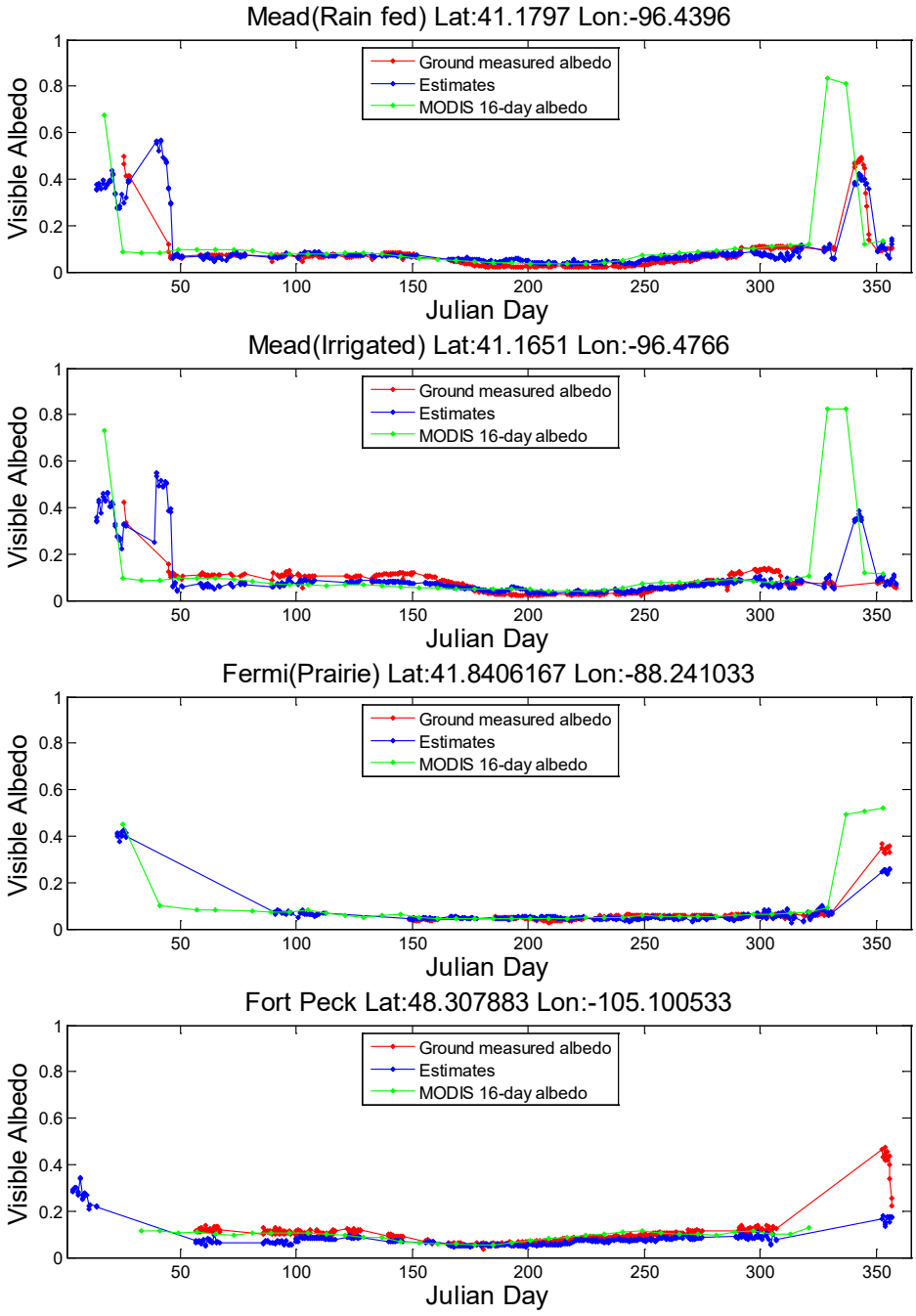

Figure 4.12. Verification of time series total visible albedo from MODIS observations in 2005 over four AmeriFlux sites (blue cross: ground measured visible albedo; red cross: estimated albedo from MODIS observations; black cross: MODIS 16-day albedo product).

Table 4.7. Statistics of the retrieved values from this study and MODIS albedo products with comparison to ground measurements over AmeriFlux sites

	Bias	STD	RMSE	R^2
Mead (Rain fed)	-0.007	0.038	0.039	0.769
Mead (Irrigated)	0.005	0.036	0.037	0.371
Fermi	0.002	0.021	0.021	0.886
Fort Peck	0.024	0.044	0.050	0.479
All sites	0.006	0.386	0.039	0.591
All sites from MODIS	-0.007	0.107	0.107	0.701

Time series comparisons of ground measurements, retrieved albedo values, and MODIS albedo products over the GC-Net sites are given in Figure 4.13. From the results shown here, snow and snow-melt events were clearly captured by the retrievals of this proposed algorithm. Variations of ground measurements and the retrieved albedo data can be found on the daily basis results whereas the 16-day MODIS albedo curves are smooth over most cases. The cause of the albedo variations is the changes in solar zenith angle, since MODIS can have multiple overpasses over Greenland in one day (combined Terra and Aqua). As more observations can be obtained over Greenland compared to those of the SURFRAD and AmeriFlux sites, the time range of collecting the cloud free observations is actually shorter over the Greenland sites, which gives the algorithm better capability capturing rapid changes. This algorithm gave a satisfying result over all sites with a small positive bias (0.012). The overall R2 (0.842) shows that the albedo retrievals have a good correlation with the ground measurements indicating that the changes of snow surfaces can be well captured, although sometimes the sliding window size is still larger than the real situation given that the RMSEs are higher than 0.05 over some sites.

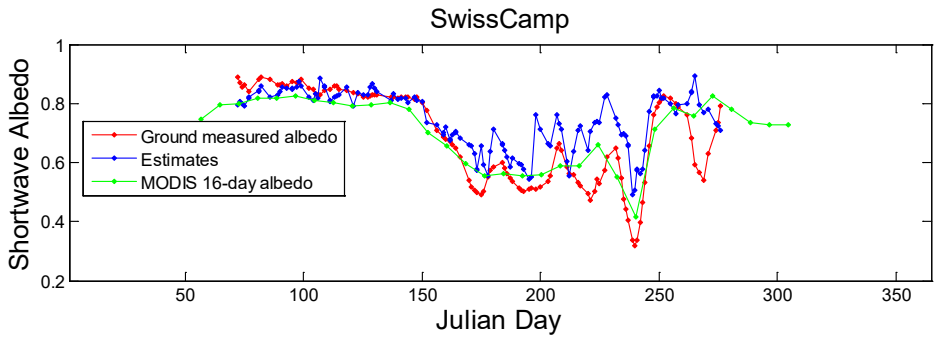
SwissCamp
Shortwave Albedo
Julian Day
Ground measured albedo
Estimates
MODIS 16-day albedo

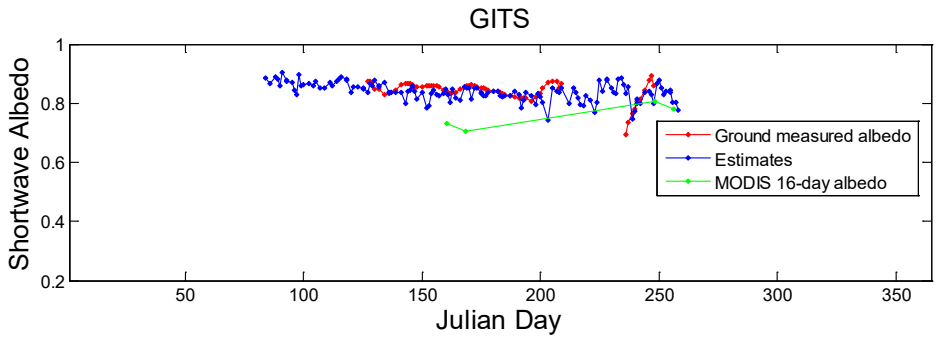
GITS
Shortwave Albedo
Julian Day
Ground measured albedo
Estimates
MODIS 16-day albedo

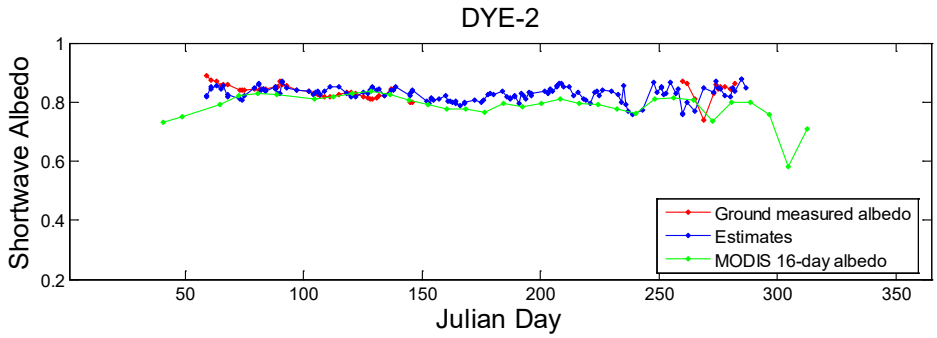
DYE-2
Shortwave Albedo
Julian Day
Ground measured albedo
Estimates
MODIS 16-day albedo

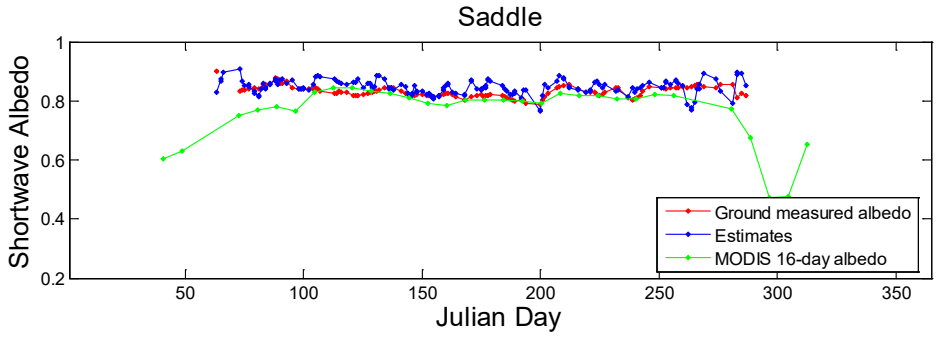
Saddle
Shortwave Albedo
Julian Day
Ground measured albedo
Estimates
MODIS 16-day albedo

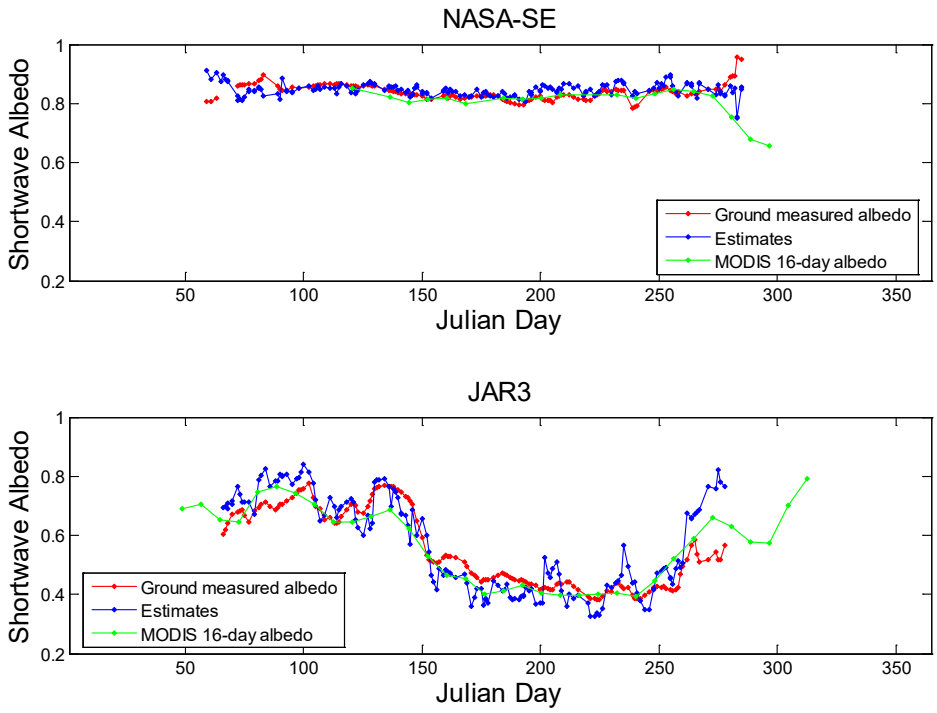

Figure 4.13. Verification of time series total shortwave albedo from MODIS observations in 2003 over six GC-Net sites (red diamond: ground measured visible albedo; blue diamond: estimated albedo from MODIS observations; green diamond: MODIS 16-day albedo product; gray cross and error bar: multiyear averaged MODIS albedo and one-year standard deviation).

Table 4.8. Statistics of the retrieved values from this study comparison to ground measurements over GC-Net sites

	Bias	RMSE	R^2
Swiss Camp	0.062	0.111	0.700
GITS	-0.011	0.036	0.077
Summit	0.010	0.047	0.027
DYE-2	-0.004	0.033	0.006
JAR1	0.015	0.091	0.872
Saddle	0.015	0.030	0.060
NASA-E	-0.024	0.034	0.002
NASA-SE	0.007	0.035	0.000
JAR3	0.001	0.077	0.774
All sites	0.012	0.065	0.842

4.2.6 Validation results of BRF

Sixteen sites are chosen in the validation of the surface reflectance using the MODASRVN data set. Time-series comparisons of the red band and near-infrared band data over six vegetation sites are given in Figure 4.14. The retrieved surface reflectances in the two bands capture the seasonal trends and match the MODASRVN instantaneous reflectance products very well. However, due to the failure to provide the reflectance over the snow covered surfaces from the MODASRVN data in most cases, it is difficult to validate the proposed algorithm over bright surfaces using this dataset. Moreover, as this dataset only relies on the MODIS sensor onboard Terra, fewer retrievals are available than our results in this study. Direct comparisons are given in Figure 4.15 over all sixteen sites for all 7 MODIS bands. The overall correlation of the retrievals and MODASRVN data is very good for each individual band and the bias and RMSE are small. The R-squared values are relatively small for band 3 and band 4 as there is only a narrow range for the reflectances (0–0.2). Some outliers are found in the comparison, probably due to the misclassification of the cloud mask, which is one of the major input components for this algorithm. Given the variability of surface cover types in all the sixteen sites, the results show that the algorithm proposed here is capable of handling different types of land cover regardless of its homogeneity.

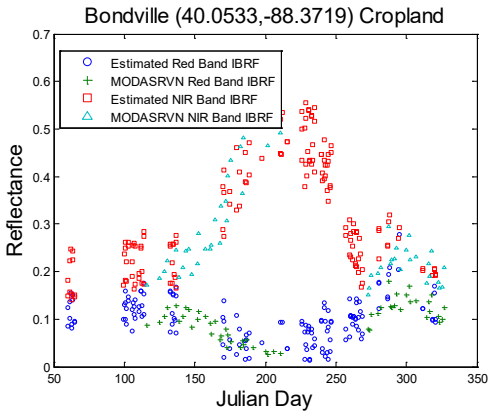

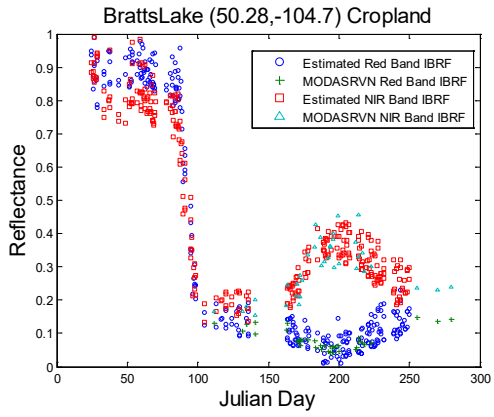

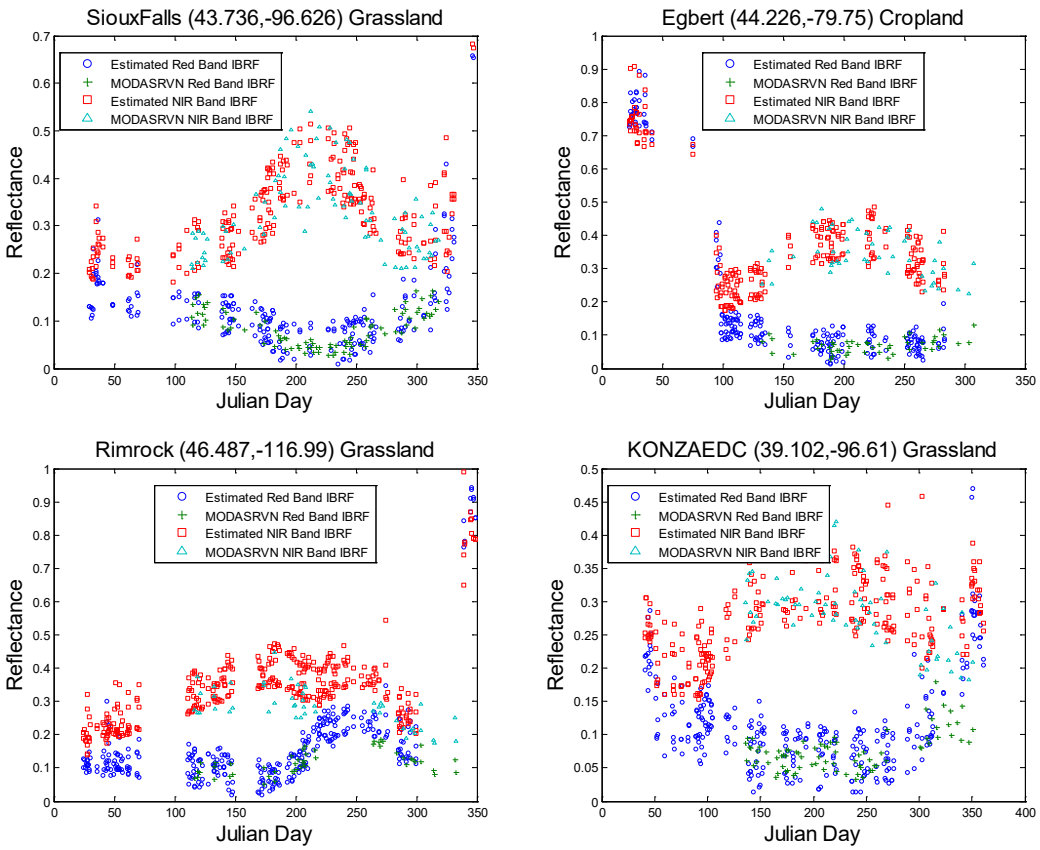

Figure 4.14. Verification of time series instantaneous reflectance from MODIS observations in 2005 over six AERONET sites (dark blue circle: estimated red band reflectance; green cross: MODASRVN red band reflectance; red square: estimated near-Infrared band reflectance; light blue triangle: MODASRVN near-Infrared band reflectance).

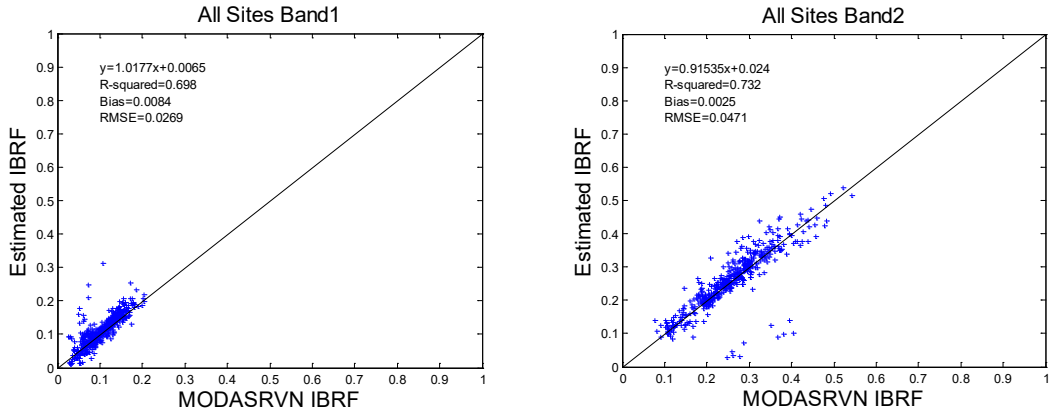

.

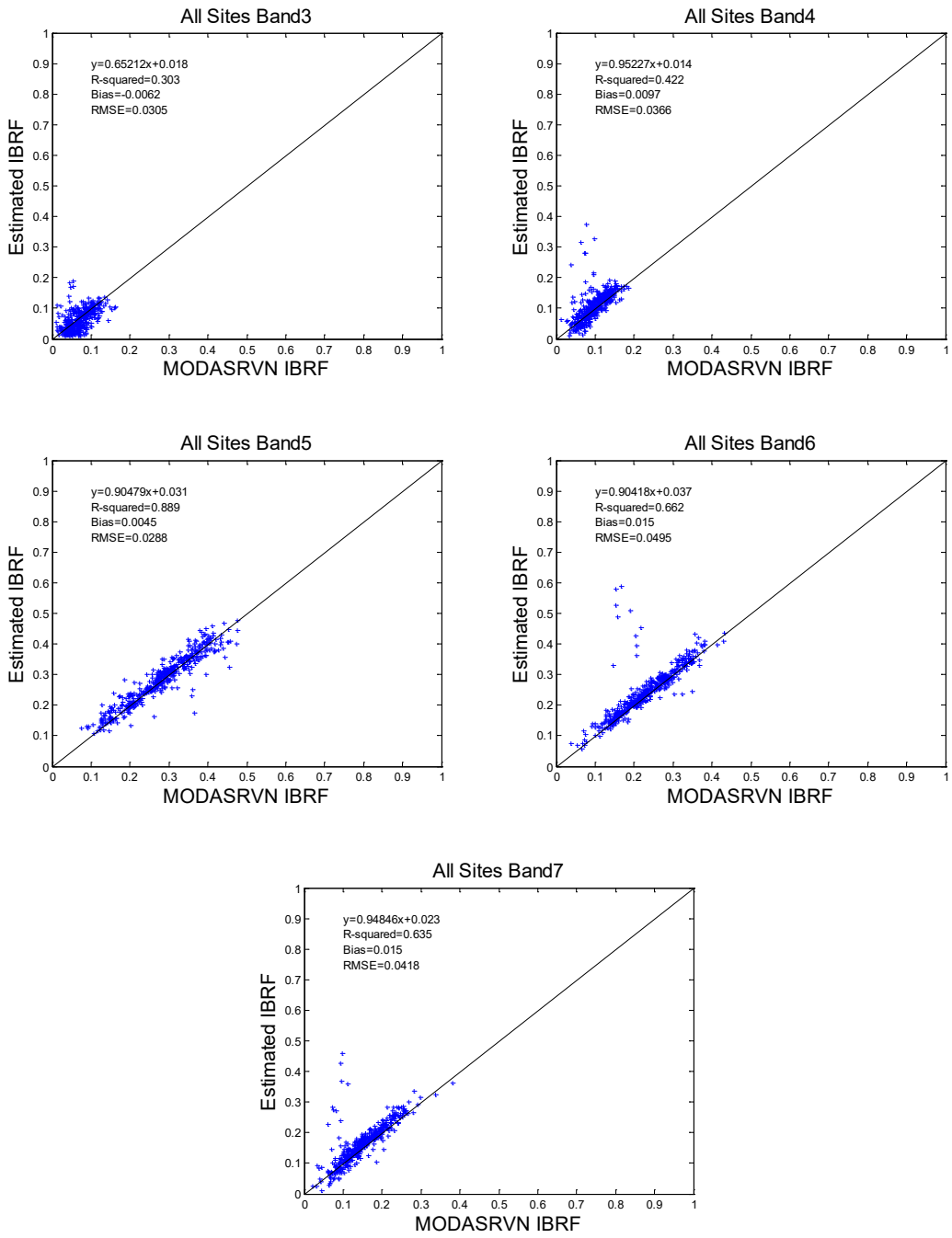

Figure 4.15. Scatter plot of estimated and MODASRVN instantaneous bidirectional reflectance for each of the seven MODIS bands over all the selected AERONET sites during 2005.

Table 4.9. Statistics of the retrieved reflectance values from this study with comparison to MODASRVN reflectance products ground measurements over sixteen AERONET sites

Band No.	Bias	RMSE	R^2
1	0.008	0.027	0.698
2	0.003	0.047	0.732
3	-0.006	0.031	0.303
4	0.010	0.037	0.422
5	0.005	0.029	0.889
6	0.015	0.050	0.662
7	0.015	0.042	0.635

4.2.7 Validation of AOD

In the offline mode, the LSA algorithm takes AOD as input and also updates AOD values in the process of optimization. Here we compare the updated AOD values from the optimization with AOD measurements at ten MODASRVN sites. Data for 500nm were transformed to 550nm in order to make the comparison with retrievals from MODIS observations. The monthly statistics of AOD were added into the surface albedo/reflectance retrieving procedure by constraining the physical range of optical depth. The overall comparison showed that the aerosol estimations have a small bias of 0.029 which means the algorithm can well capture the aerosol information in the TOA signals (Figure 4.16). However, there were some over- and under-estimations which deteriorated the RMSE to 0.1 when either the real AOD values fell out of the major monthly distribution or a large variation of AOD was found for that particular time period.

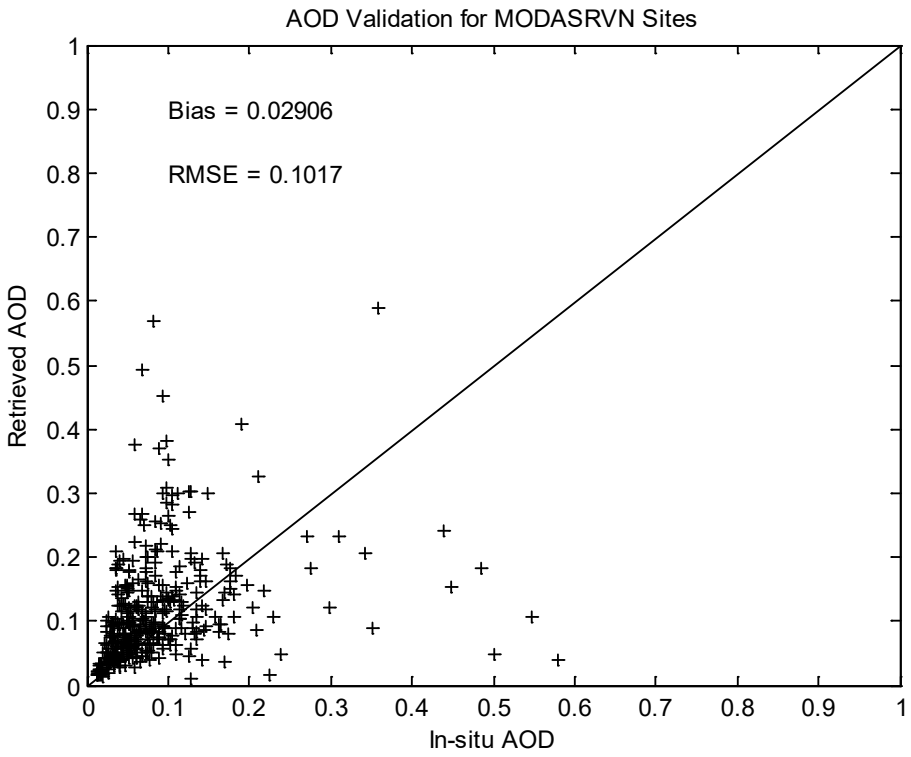

Figure 4.16. Validation summary of AOD at 550nm over MODASRVN sites for the year of 2005.

4.2.8 Summary of Accuracy and Precision

The statistics of albedo validation is given in two groups: non-snow surfaces and snow surfaces. Non-snow surfaces use the data from SURFRAD sites and snow surfaces include sites of GC-Net. The performance of the LSA algorithm over both surfaces satisfies the requirements of F&PS in terms of precision and accuracy. The listed accuracy requirement for ABI albedo is 0.08 albedo unit and the error (RMSE) of our retrievals is 0.01 over both surfaces. In terms of RMSE (precision), we achieve a value of 0.06 over non-snow sites and 0.07 over snow sites while the F&PS requirement is 10% (Table 4.10). For the real ABI data, we expect even higher accuracy, since the ABI data have a temporal resolution of 15 minutes, providing sufficient data within a shorter time period, which is extremely important for the cases of rapidly changing surface properties, such as transitions between snowfall and snow melting.

Table 4.10. Summary of albedo validation results

	Non-snow	Snow	F&PS Requirement
Accuracy(Bias)	0.01	0.01	0.08
Precision(RMSE)	0.06	0.07	10%
R2	0.82	0.84	N/A

Statistics of validation results of BRF over red and NIR bands are summarized in Table 4.11. The bias of our estimate is well below the requirement. In terms of RMSE (precision), our retrievals over all bands are also below 0.05.

Table 4.11. Summary of BRF validation results

	Red Band	NIR Band	Requirement
Accuracy(Bias)	0.008	0.003	0.08
Precision(RMSE)	0.027	0.047	5%
R^2	0.698	0.732	N/A

4.3 Validation using local GOES-R ABI Albedo/Reflectance Data

4.3.1 Validation dataset

Around one year's data from ABI (October 2017–September 2018) observations were processed for evaluation and validation purpose at 1-km scale. TOA observations from the early morning or late afternoon (solar zenith angle larger than 75°) were not used to retrieve surface albedo.

Ground measurements were used to validate the surface albedo and reflectance estimated from the geostationary satellites, including flux data from the Surface Radiation Budget Network (SURFRAD) sites and the OzFlux sites, as well as aerosol observations from the Aerosol Robotic Network (AERONET) sites. For details of this validation attempts refer to He et al. (2019), and some main results are listed here.

4.3.2 Validation result

The validation work has performed two analyses in evaluating the ABI-based albedo estimation. First the hourly ABI albedo was validated against SURFRAD site measurements at the daily temporal resolution.

Table 4.12 shows the validation statistics of hourly clear-sky surface albedo against ground measurements. Generally, the ABI surface albedo estimation had a very small bias with an RMSE of 0.050 and a relative RMSE (RMSE of the relative difference between satellite retrievals and ground measurements) of 19.8%. Five sites have absolute bias values lower than 0.010. The largest RMSE was found at the Bondville site, which is an agriculture site in Illinois, US, with spatial heterogeneity issues from the ephemeral snow events and the wet drainage system around the site.

Table 4.12 ABI albedo validation results at SURFRAD sites

Site	Hourly		Local solar noon	
	Bias	RMSE	Bias	RMSE
Fort Peck	0.005	0.049	0.004	0.04
Sioux Falls	-0.005	0.046	-0.004	0.032

Penn State	-0.009	0.053	-0.012	0.036
Bondville	-0.008	0.072	-0.018	0.045
Boulder	0.011	0.054	0.008	0.035
Desert Rock	0.012	0.033	-0.003	0.017
Goodwin Creek	-0.007	0.032	-0.009	0.027
All	-0.000	0.05	-0.004	0.032

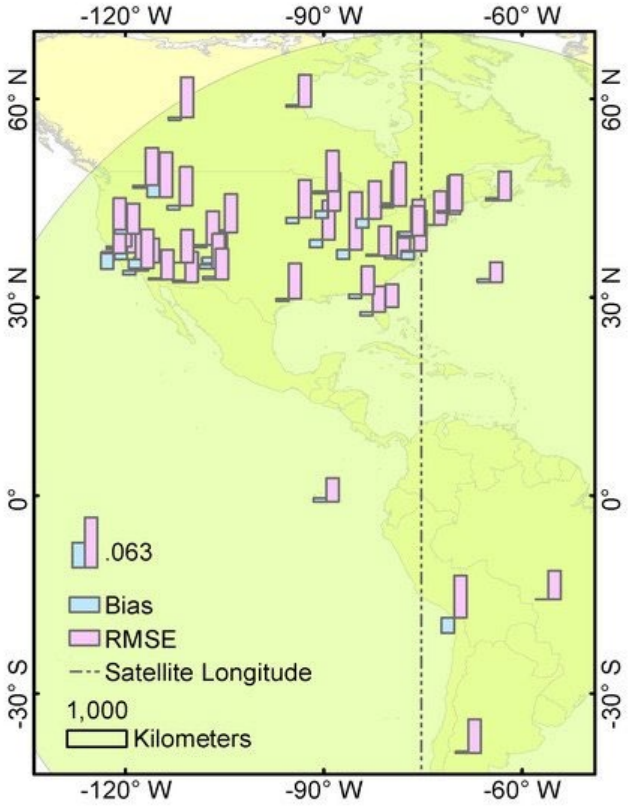

Figure 4.17 ABI reflectance validation results at AERONET sites. The blue and pink bars represent the validation bias and RMSE for each of the AERONET sites. The green circle represents the satellite coverage with the maximum view zenith angle of 70°. The dash-dotted line represents the central longitude of GOES-16. The length of the vertical pink legend represents the value equivalent to 0.063.

In the validation of local noon albedos (Table 4.12), the ABI albedo provides an overall RMSE of 0.032. Figure 4.17 show the reflectance validation results against AERONET AOD corrected surface reflectance values. The ABI surface reflectance agrees well with atmospherically corrected surface reflectance. The overall RMSE is 0.042 with a bias very close to zero. The site-level bias and RMSE ranges from −0.019 to 0.015 and from 0.025 to 0.072, respectively. Most of the sites have absolute bias and RMSE below 0.010

and 0.050, respectively. There does not seem to be any obvious spatial pattern of bias and RMSE in Figure 4.17.

4.4 Comparison of reflectance with MODIS simulated counterparts

Since MODIS and GOES-R has different observing geometry, it is difficult to find sufficient counterparts from MODIS surface reflectance and GOES-R surface reflectance directly under some large angle conditions. However, the MODIS BRDF (MCD43A1 used here) is supposed to depict the surface anisotropy and could predict the surface reflectance under specific angles. Thus we could compare GOES-R surface reflectance with MODIS simulated surface reflectance under identical solar/view geometry to evaluate the performance of GOES-R reflectance. Here we chose an experimental area in West CONUS (Figure 4.18), with large view zenith angle in GOES-R observations. In order to minimize differences due to the spectral response, the bands used for comparison were those that correspond most closely between the different instruments. The band correspondence is given in figure captions. Noted that the data used in this version is the operational product corresponding to v2.2.5. The R2 derived surface reflectance would have a better quality after deploying the BRDF climatology in v3.

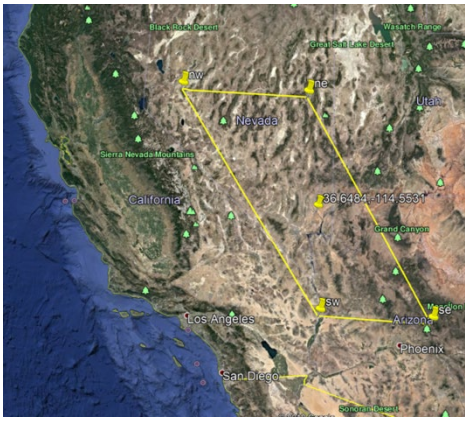

Figure 4.18 Test area in Surface reflectance comparison with MODIS predictions.

There is a certain amount of scatter evident in all scatter plots shown in Figure 4.19, while the distribution plot also shows some deviation, but the regions shown as darker red, representing the majority of the pixels, are much less scattered. This is supported by the bias, which are all in the range 0.00 to 0.04 in the R3 retrievals of different bands. The R2 retrievals have higher bias which implies the difference in the BRDF retrievals, which would be reduced in the updated result in v2.3. R3 is the subroutine for the majority of the clear-sky observations, and the shown sample represents the worst case that could be dobserved in the GOES-R reflectance product as the VZA has reached 60°.

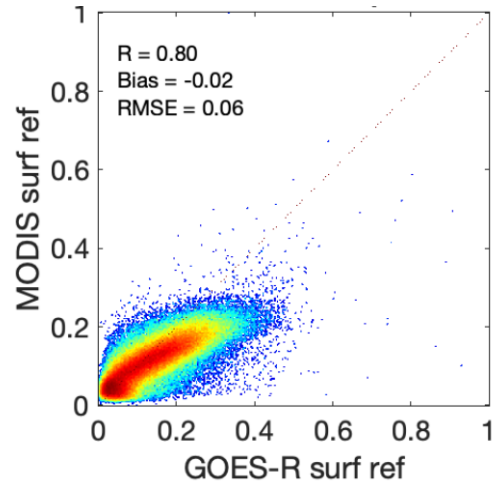

(a) GBand1_Mband3_R2

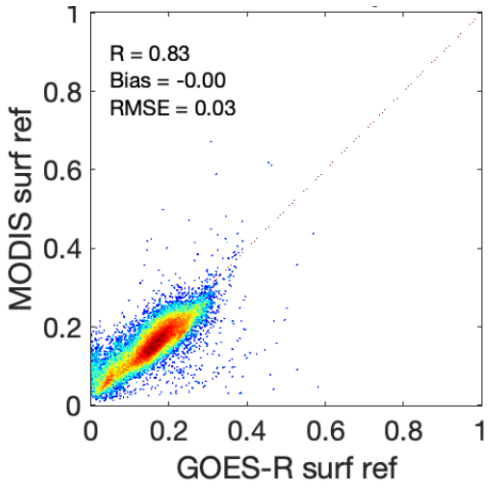

(b) GBand1_Mband3_R3

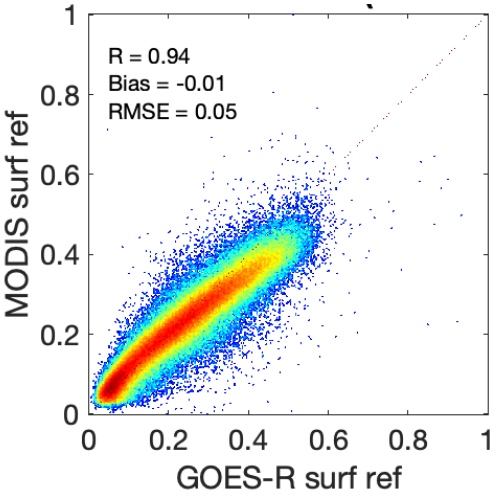

(c) GBand2_Mband1_R2

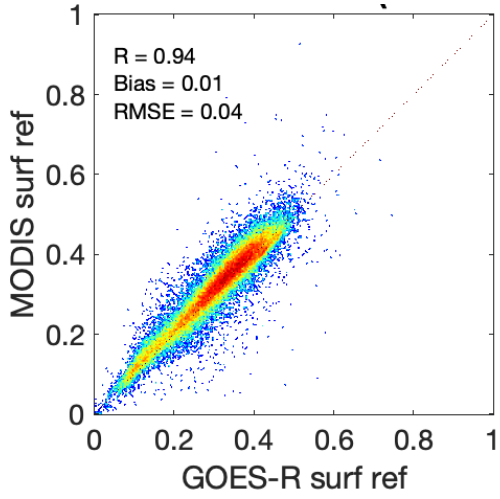

(d) GBand2_Mband1_R3

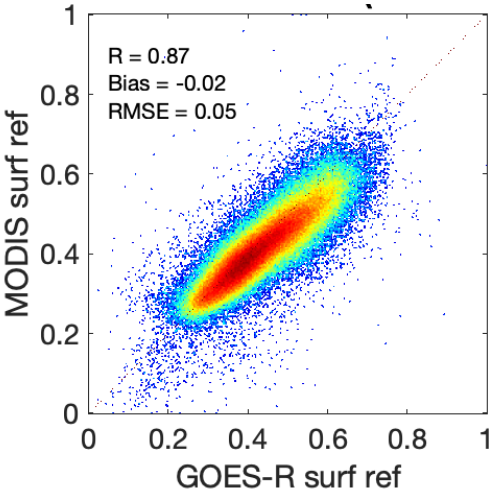

(e) GBand3_Mband2_R2

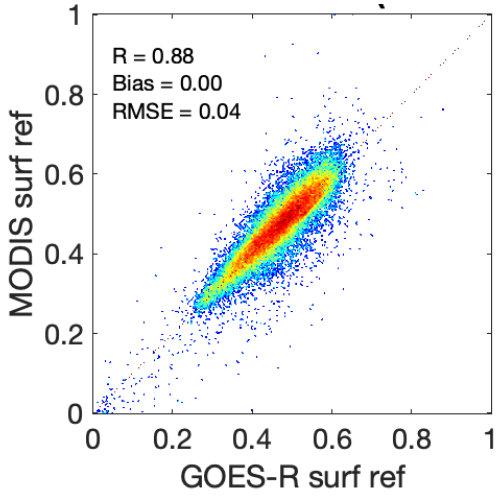

(f) GBand3_Mband2_R3

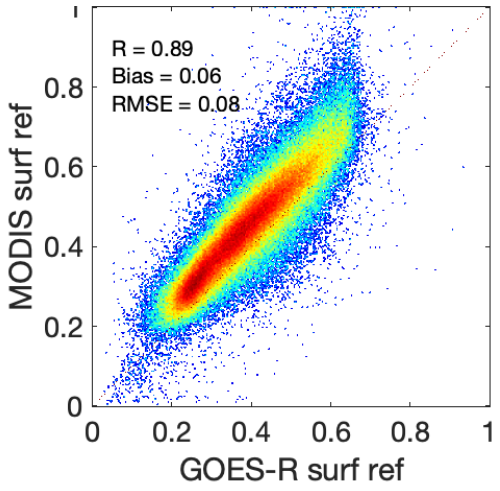

(g) GBand5_Mband6_R2

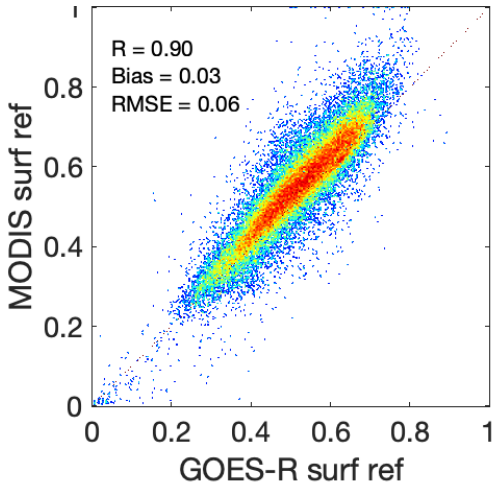

(h) GBand5_Mband6_R3

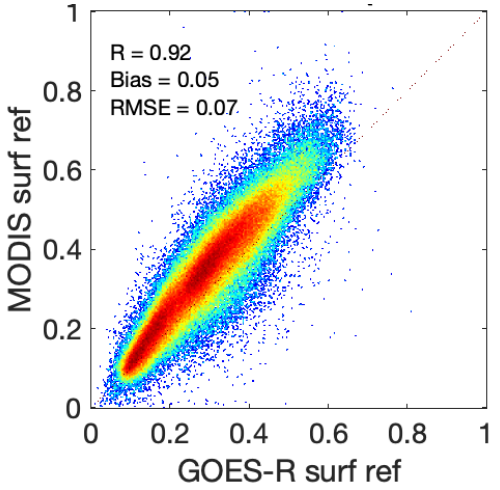

(i) GBand6_Mband7_R2

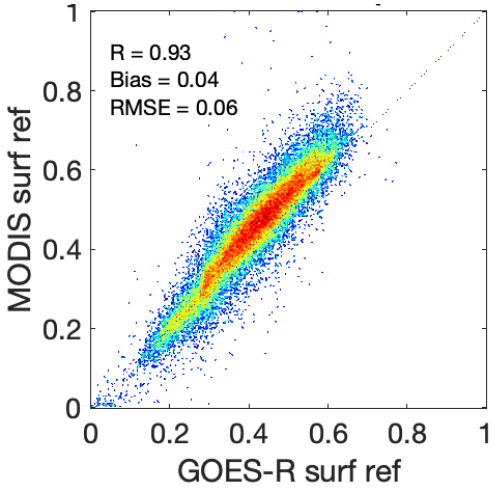

(j) GBand6_Mband7_R3

Figure 4.19. Comparison of GOES-R surface reflectance at each band with MODIS counterparts simulated from MCD43A1 BRDF using the GOESR observing angles at 17:30 UTC on Oct 17, 2019. Comparison is conducted over samples from R2 and R3 respectively.

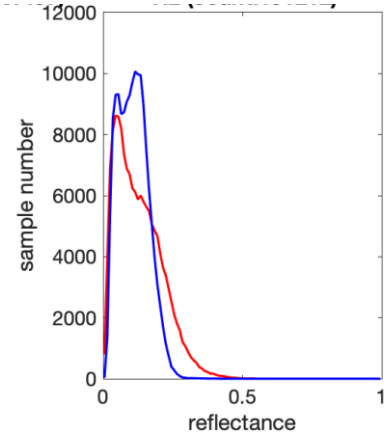

(a) GBand1_Mband3_R2

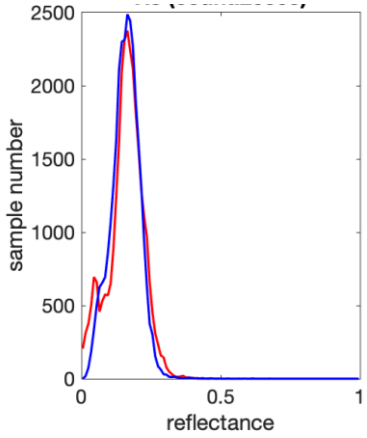

(b) GBand1_Mband3_R3

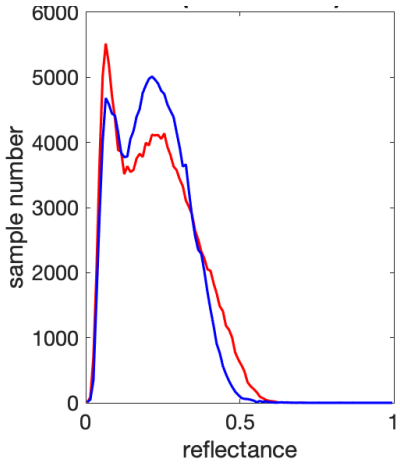

(c) GBand2_Mband1_R2

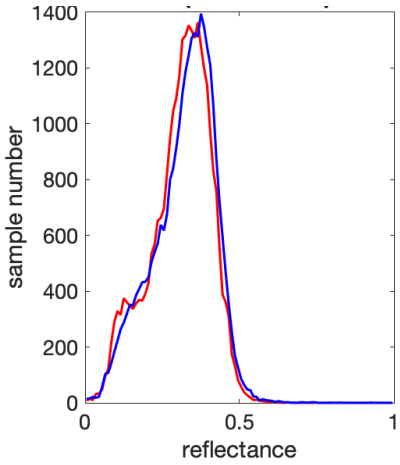

(d) GBand2_Mband1_R3

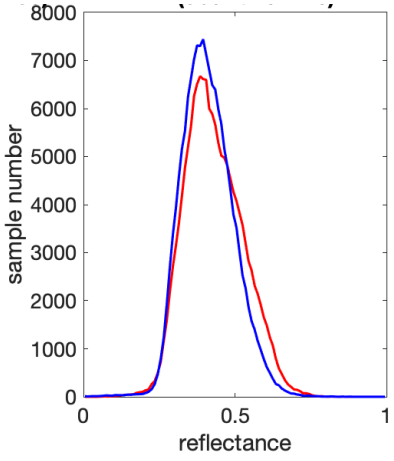

(e) GBand3_Mband2_R2

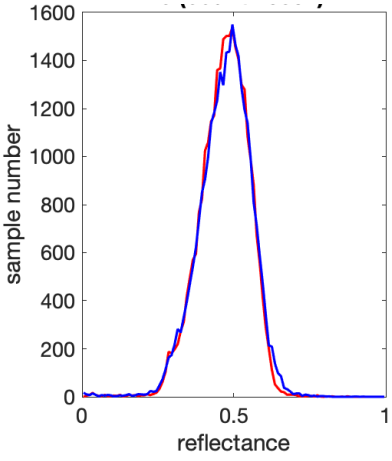

(f) GBand3_Mband2_R3

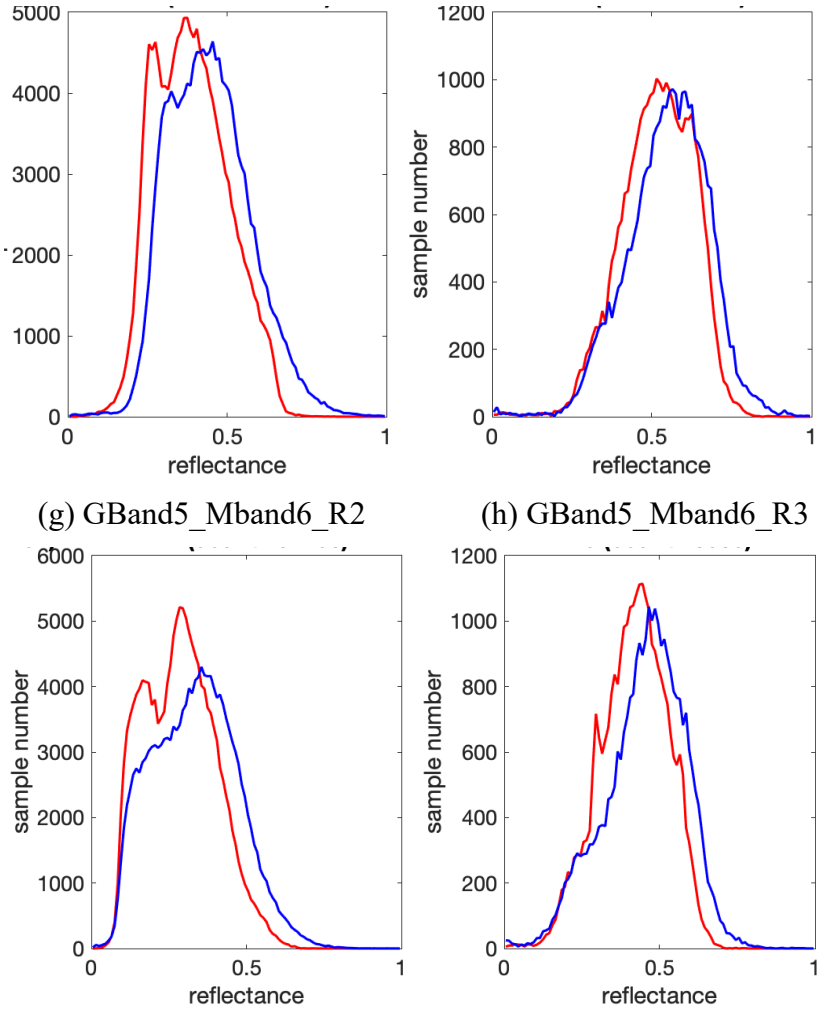

(g) GBand5_Mband6_R2 (h) GBand5_Mband6_R3

(i) GBand6_Mband7_R2 (j) GBand6_Mband7_R3

Figure 4.20. Distribution of GOES-R surface reflectance at each band with MODIS counterparts simulated from MCD43A1 BRDF using the GOESR observing angles at 17:30 UTC on Oct 17, 2019.

5 PRACTICAL CONSIDERATIONS

5.1 Numerical Computation Considerations

Accurate retrieval of albedo requires reliable acquisition of atmospheric parameters. Forward running of atmospheric radiative transfer model is time-consuming and not suitable for operational retrieval of albedo. Instead, the LSA algorithm pre-runs the atmospheric radiative transfer at some given conditions and stores the parameters into the LUTs to save computational time.

The current version of the LSA algorithm includes an optimization process. To speed up the iterative process, we may have to limit the number of iterations or adjust the iteration convergence criteria. Moreover, the optimization procedure takes advantage of multiple processor cores to perform parallel block processing on large FD image to reduce the latency. The default number of processes is 24.

5.2 Programming and Procedural Considerations

The LSA algorithm is purely a pixel-by-pixel algorithm. However, it requires a time series of clear-sky observations to achieve enough information to inverse BRDF models. Given the data volume of full disk albedo products, it is inefficient to gather a stack time series data over all pixels at each ABI scanning time. Given that the BRDF parameters do not vary greatly over a short period of time, we use the pre-calcualted BRDF parameters from the previous day to save computational time. In order to achieve this, we divide our algorithm into two parts, online and offline modes, respectively.

5.3 Quality Assessment and Diagnostics

The retrieval process of albedo will be monitored and the retrieval quality will be assessed. A set of quality flags and metadata will be generated with the albedo product for retrieval diagnostics. These flags will indicate the retrieval conditions, including the land/water mask, solar zenith angle and local zenith angle ranges. These flags also indicates the data quality (Is the data quality of AOD available? Is a routine BRDF retrieval algorithm successful? Which path is used to calculate LSA and BRF). The detailed information is documented in Section 3.5.

5.4 Exception Handling

The LSA algorithm checks for conditions where the albedo retrieval cannot be performed. These conditions include the failure of sensors, such as saturated channels or missing values. They also include the conditions when continuous clouds are present so that there are no enough clear-sky observations. However, the LSA algorithm tries to avoid using filling values if possible, in order to produce continuous and consistent products. The LSA algorithm selects various paths to calculate albedo and BRF in the online mode. The filling value of BRF is used only when no BRDF parameter is retrieved and the current observation is cloudy. The LSA algorithm cannot run without cloud mask. However, if

there is no AOD available, the offline mode is still able to run normally and the online mode will use a default AOD value to calculate diffuse irradiance ratio and carry out atmospheric correction.

5.5 Algorithm Validation

A summary of our previous validation results has been given in Section 4. In order to quantify the retrieval errors and improve the inversion algorithm, we need to carry out more extensive validation work before and after launch of the GOES-R satellite. Albedo is continuously measured by several surface measurement networks, such as Atmospheric Radiation Measurement at the Southern Great Plains, SURFRAD, and Ameriflux projects. Albedo measurements at more than a hundred sites are available for pre-launch and post-launch validation. We have conducted albedo validation extensively during recent years (Chen et al. 2008; Liang et al. 2002; Liang et al. 2005b).

However, the actual GOES_R ABI albedo performance is not as expected in the first several months after launched, due to the large uncertainty in the BRDF coefficients generated in offline process. Main reasons include the carryover effect of an dissatisfied initial value and search range, which was determined by the BRDF coefficients from the previous day. In another word, when the BRDF quality is influenced by inadequate observations or outliers in one day, it will be transferred to the following day through regulating the initial value and search range of BRDF in the optimization process. As a mitigation in the V2.5, the algorithm has deployed the BRDF climatology instead of the previous day's BRDF to as prior knowledge in the BRDF optimization. Moreover, before the updated BRDF are fully evaluated, we also done some adjustments in the online processing to improve the product performance. The R1 subroutine has been temporally disabled since it relies on the BRDF coefficients to do the atmospheric correction and the negative effects from BRDF outweigh the positive benefits. The Lambertian atmospheric correction is assigned as the main subroutine instead and its performance has been evaluated through cross-comparison with MODIS data. By using the 4-level cloud mask to recognize the clear-sky observations, the surface reflectance of 'probably clear' pixels will also be obtained from atmospheric correction rather than previous BRDF simulation in the V2.3.

Noted that spatial effects of validation LSA products have not been well addressed in current ATBD. The scale effect or the change of support is always a problem in validating satellite land products, especially those of moderate or coarse resolutions. Due to the practical challenges and the availability of measurements, in situ measurements of albedo from pyranometers are directly compared with satellite retrievals of albedo in our current validation activities and many other published investigations of albedo validation. We've noticed this problem. The scale effect has to be accounted in order to better evaluate accuracy and precision of GEOS-R albedo products. We have submitted a GOES-R cal/val proposal entitled "validating GOES-R land surface shortwave radiation products" to further investigate this issue.

6 ASSUMPTIONS AND LIMITATIONS

The following sections describe the assumptions in developing and estimating the performance of the current version of ABI LSA algorithm. The limitations and potential algorithm improvement are also discussed.

6.1 Performance

The following assumptions have been made in developing and estimating the performance of the ABI LSA algorithm:

- Surface BRF is modeled by the revised linear kernel function with three coefficients.
- Surface anisotropy is constant within days through a moving window and can be represented by the linear kernel model.
- The reciprocity principle is valid at ABI resolutions.
- The systematic bias caused by lambertian assumption is acceptable. It is assumed to cause an underestimation of surface reflectance when BRDF is high and overestimation when BRDF is low.

6.2 Assumed Sensor Performance

The ABI LSA algorithm requires a time series of clear sky TOA reflectance inputs. The number of clear sky observations within a short time period will influence the retrieval quality of LSA and corresponding land surface reflectance by-products. Additionally, the algorithm relies on the cloud mask product to distinguish clear-sky observations from cloud sky observations. The retrieval accuracy also depends on the quality of cloud mask.

6.3 Algorithm Improvement

The introduction of prior knowledge such as the aerosol types, BRDF models, BRDF climatology, and albedo climatology will improve the retrieval quality of LSA and land surface reflectance. Currently, we use the multi-year's mean and variance of MODIS albedo products as one of the constraints in our optimization code. We are currently working on analyzing more existing satellite albedo/BRDF products and in an effort to incorporate as much background knowledge as possible. Moreover, we are considering to develop an AOD climatology for improving the offline optimization efficiency and online albedo and reflectance accuracy.

7 REFERENCES

Chen, Y.M., Liang, S., Wang, J., Kim, H.Y., & Martonchik, J.V. (2008). Validation of MISR land surface broadband albedo. *International Journal of Remote Sensing, 29*, 6971-6983

Duan, Q.Y., Gupta, V.K., & Sorooshian, S. (1993). Shuffled complex evolution approach for effective and efficient global minimization. *Journal of Optimization Theory and Applications, 76*, 501-521

Duan, Q.Y., Sorooshian, S., & Gupta, V. (1992). Effective and efficient global opitimization for conceptual rainfall-runoff models. *Water Resources Research, 28*, 1015-1031

Govaerts, Y.M., Wagner, S., Lattanzio, A., & Watts, P. (2010). Joint retrieval of surface reflectance and aerosol optical depth from MSG/SEVIRI observations with an optimal estimation approach: 1. Theory. *Journal of Geophysical Research-Atmospheres, 115*

He, T., Liang, S.L., Wang, D., Wu, H., Yu, Y., & Wang, J. (2012). Estimation of surface albedo and directional reflectance from Moderate Resolution Imaging Spectroradiometer (MODIS) observations. *Remote Sensing of Environment, 119*, 286-300

He, T., Zhang, Y., Liang, S., Yu, Y., & Wang, D. (2019). Developing Land Surface Directional Reflectance and Albedo Products from Geostationary GOES-R and Himawari Data: Theoretical Basis, Operational Implementation, and Validation. *Remote Sensing, 11(22), 2655.*

Liang, S., Yu, Y., & Defelice, T.P. (2005a). VIIRS narrowband to broadband land surface albedo conversion: formula and validation. *International Journal of Remote Sensing, 26*, 1019-1025

Liang, S.L. (2001). Narrowband to broadband conversions of land surface albedo I Algorithms. *Remote Sensing of Environment, 76*, 213-238

Liang, S.L. (2003). A direct algorithm for estimating land surface broadband albedos from MODIS imagery. *Ieee Transactions on Geoscience and Remote Sensing, 41*, 136-145

Liang, S.L. (2004). *Quantitative remote sensing of land surfaces*. Hoboken, New Jersey: John Wiley & Sons, Inc

Liang, S.L., Fang, H.L., Chen, M.Z., Shuey, C.J., Walthall, C., Daughtry, C., Morisette, J., Schaaf, C., & Strahler, A. (2002). Validating MODIS land surface reflectance and albedo products: methods and preliminary results. *Remote Sensing of Environment, 83*, 149-162

Liang, S.L., Shuey, C.J., Russ, A.L., Fang, H.L., Chen, M.Z., Walthall, C.L., Daughtry, C.S.T., & Hunt, R. (2003). Narrowband to broadband conversions of land surface albedo: II. Validation. *Remote Sensing of Environment, 84*, 25-41

Liang, S.L., Strahler, A.H., & Walthall, C. (1999). Retrieval of land surface albedo from satellite observations: A simulation study. *Journal of Applied Meteorology, 38*, 712-725

Liang, S.L., Stroeve, J., & Box, J.E. (2005b). Mapping daily snow/ice shortwave broadband albedo from Moderate Resolution Imaging Spectroradiometer (MODIS): The improved direct retrieval algorithm and validation with Greenland in situ measurement. *Journal of Geophysical Research-Atmospheres, 110*

Maignan, F., Breon, F.M., & Lacaze, R. (2004). Bidirectional reflectance of Earth targets: Evaluation of analytical models using a large set of spaceborne measurements with emphasis on the Hot Spot. *Remote Sensing of Environment, 90*, 210-220

NOAA (2009). GOES-R Series Ground Segment Project Functional and Performance Specification. In

Pinty, B., Roveda, F., Verstraete, M.M., Gobron, N., Govaerts, Y., Martonchik, J.V., Diner, D.J., & Kahn, R.A. (2000a). Surface albedo retrieval from Meteosat - 1. Theory. *Journal of Geophysical Research-Atmospheres, 105*, 18099-18112

Pinty, B., Roveda, F., Verstraete, M.M., Gobron, N., Govaerts, Y., Martonchik, J.V., Diner, D.J., & Kahn, R.A. (2000b). Surface albedo retrieval from Meteosat - 2. Applications. *Journal of Geophysical Research-Atmospheres, 105*, 18113-18134

Qin, W.H., Herman, J.R., & Ahmad, Z. (2001). A fast, accurate algorithm to account for non-Lambertian surface effects on TOA radiance. *Journal of Geophysical Research-Atmospheres, 106*, 22671-22684

Schaaf, C., Martonchik, J., Pinty, B., Govaerts, Y., Gao, F., Lattanzio, A., Liu, J., Strahler, A., & Taberner, M. (2008). Retrieval of Surface Albedo from Satellite Sensors. In S. Liang (Ed.), *Advances in Land Remote Sensing: System, Modeling, Inversion and Application* (pp. 219-243). New York: Springer

Schaaf, C.B., Gao, F., Strahler, A.H., Lucht, W., Li, X.W., Tsang, T., Strugnell, N.C., Zhang, X.Y., Jin, Y.F., Muller, J.P., Lewis, P., Barnsley, M., Hobson, P., Disney, M., Roberts, G., Dunderdale, M., Doll, C., d'Entremont, R.P., Hu, B.X., Liang, S.L., Privette,

J.L., & Roy, D. (2002). First operational BRDF, albedo nadir reflectance products from MODIS. *Remote Sensing of Environment, 83*, 135-148

Wagner, S.C., Govaerts, Y.M., & Lattanzio, A. (2010). Joint retrieval of surface reflectance and aerosol optical depth from MSG/SEVIRI observations with an optimal estimation approach: 2. Implementation and evaluation. *Journal of Geophysical Research-Atmospheres, 115*

Wang, D., Liang, S.L., He, T., & Yu, Y. (2013). Direct estimation of land surface albedo from VIIRS data: algorithm improvement and preliminary validation. *Journal of Geophysical Research-Atmospheres, 118*, 12,577-512,586

Wang, Y.J., Lyapustin, A.I., Privette, J.L., Morisette, J.T., & Holben, B. (2009). Atmospheric Correction at AERONET Locations: A New Science and Validation Data Set. *Ieee Transactions on Geoscience and Remote Sensing, 47*, 2450-2466

Yang, F.L., Mitchell, K., Hou, Y.T., Dai, Y.J., Zeng, X.B., Wang, Z., & Liang, X.Z. (2008). Dependence of Land Surface Albedo on Solar Zenith Angle: Observations and Model Parameterization. *Journal of Applied Meteorology and Climatology, 47*, 2963-2982